Advances in Colloid and Interface Science 349 (2026) 103755

Contents lists available at ScienceDirect

Advances in Colloid and Interface Science

journal homepage: www.elsevier.com/locate/cis

Electrokinetic transport in saturated and unsaturated porous media: A pore-scale view☆

Yunfan Huang, Zhiguo Tian, Hangyu Chen, Wei Liu, Moran Wang *

Department of Engineering Mechanics and ASP, Tsinghua University, Beijing, 100084, China

ARTICLE INFO

Keywords:
Electrokinetics
Porous media
Interfacial transport
Multiscale simulation
Multiphysical coupling

ABSTRACT

Electrokinetic transports in porous media play a crucial role in diverse applications such as geophysical exploration, nuclear waste disposal, water desalination, soil and groundwater remediation, low-salinity waterflooding, and ionic battery operation. This review systematically examines electrokinetic mechanisms in single-phase and multiphase flows in porous media, with a special focus on multiscale and multiphysico-chemical coupling effects. After briefly introducing fundamental theories on microscale electrokinetic transports, we highlight the impact of nanoscale confinement and geometric regulation at first on single-phase electrokinetic flows and ion transport. Next, we discuss the influences of non-uniform ionic concentration and temperature fields on electrokinetic transports, encompassing the impact of surface chemical reactions via charge regulation and reactive transports, and thermodiffusion effects. Furthermore, we provide a concise overview of the current understanding of electrokinetics in multiphase flows, including interfacial charging, wettability alteration, and electrokinetic multiphase dynamics. Finally, we try to outline future research directions, addressing statistics-based theories, multiscale simulations, and advanced experimental designs for electrokinetic transports in porous media.

Contents

☆ This article is part of a Special issue entitled: 'Interfaces and fluids' published in Advances in Colloid and Interface Science.

* Corresponding author.
E-mail address: mrwang@tsinghua.edu.cn (M. Wang).

https://doi.org/10.1016/j.cis.2025.103755

Available online 12 December 2025

Nomenclature

REV	Representative elementary volume
EOF	Electroosmotic flow
PB	Poisson–Boltzmann
EDL	Electrical double layer
ETL	Electrical triple layer
EQL	Electrical quad layer
ESC	Extended space charge
C-S-H	Calcium-silicate-hydrate
RGG	Random generation-growth
QSGS	Quartet structure generation set
LBM	Lattice Boltzmann method
LPBM	Lattice Poisson–Boltzmann method
AMR	Adaptive mesh refinement
MD	Molecular dynamics
P^3M	Particle–particle particle-mesh

1. Introduction

Electrokinetic transport refers to the coupled ion-fluid motion in electrolyte solutions near charged interfaces [1,2], representing an interface-driven process from a macroscopic point of view. Porous media, with their high surface-to-volume ratios, create ideal environments for electrokinetic transport that is governed by unique effects including solid-structure confinements, interfacial/bulk multiphysical coupling, and/or soft-interface multiphase percolation.

Electrokinetic processes in porous media is ubiquitous in nature and industry. There are a few existing excellent review papers or monographs on single-phase transport in saturated porous media in different disciplines: fundamental theories [3–5], colloid/membrane science [1,6–8], soil and groundwater remediation [9–11], geological characterization [12], transpiration-driven energy harvesting [13–16], electrochemistry [17,18], and microfluidic experiments [19–22]. This paper will not repeat those but highlight new progresses that are very crucial but have not been addressed yet for single-phase electrokinetic transport, from the perspectives of two categories of effects, i.e., wall confinements and field inhomogeneity. The former focuses on the geometrical and structural factors, including discrete particle effects, geometric regulation, and spatio-temporal multiscale effects, while the latter emphasizes the coupling of different physical fields (especially those between interface and solution), where the charge regulation, kinetic transport, and temperature gradient are addressed.

On the other hand, there are examples of electrokinetic effects on multiphase flow and charge transport in unsaturated porous media [12,23–27], spanning the energy, resources, and environmental sectors. These include regulation of gas-water interfaces in fuel cells [28], directional droplet enrichment [29,30], organic spill remediation [31,32], residual oil mobilization [33–35], and geological and biological sensing [36–38]. Basically, applied electric fields can directly drive spontaneously charged interfaces while simultaneously regulating displacement through electrowetting effects that modify interfacial tension and contact angles. Besides, the equilibrium contact angle near the three-phase contact line, when mediated by disjoining pressure in nanoscale thin liquid films, is strongly affected by local ion concentration — a phenomenon termed ion-tuned wettability. Though there have been several reviews mentioning the fundamental issues such as two-liquid interface charging and electrochemical wettability alteration [24,39], the mixed interface charging mechanism and the impact of interface chemical physics on two-phase porous flow have not been systematically reviewed yet.

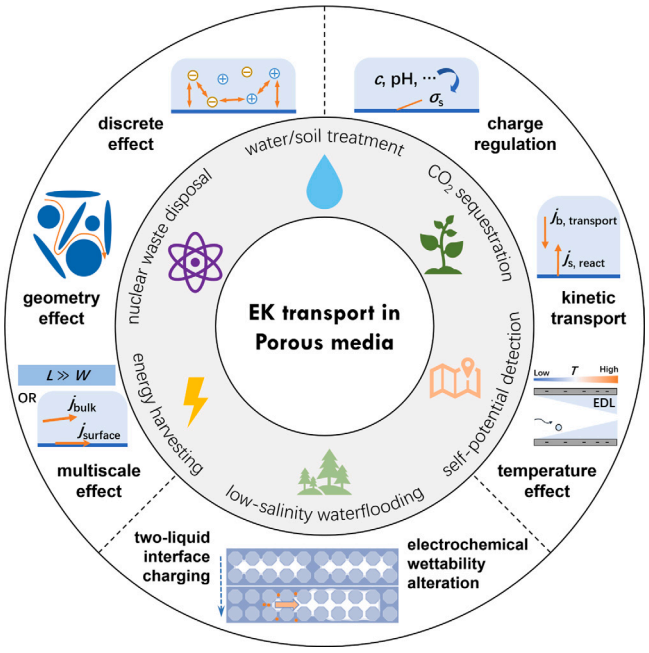

Fig. 1. Overview of the applications and mechanisms covered in this review.

In this review paper, we will focus on the pore-scale electrokinetic transport in porous media composed of perfect dielectric material, especially those systems with essentially reactive solid surface, external temperature gradient, various confinements triggered by a tiny solid channel, diffuse nature of two-liquid interface, or thin fluid film, as illustrated in Fig. 1. To ensure quantitative predictability, we introduce the appropriate fundamental numerical methods. Despite considering diverse aspects of electrokinetic transport in porous media, the topics and views (as shown in Fig. 1) are still constrained by the authors' limited research expertise and experience, which primarily employs multiscale modeling and simulations. The review is structured as follows. Sections 2 and 3 detail electrokinetic transport in saturated porous media, while Section 4 provides a concise overview of unsaturated porous systems. Conclusions and future perspectives are presented in Section 5.

2. Electrokinetic transport in saturated porous media: effect of wall confinements

Electrokinetic transport occurs near the interfaces, making porous media (with numerous interfaces inside) ideal for electrokinetic regulation. In early days, the thickness of the electric double layer (EDL) was assumed to be thin enough compared with the channel width or pore size [1]. Thus, in a simple channel geometry or for those potential flows in porous media with $\mathrm{Re} \ll 1$, the EOF can be well characterized by the so-called Helmholtz-Smoluchowski model, where the EOF velocity is determined by [1]

$$u_{\mathrm{HS}} = \frac{\varepsilon\zeta}{\mu}\nabla\varphi. \tag{1}$$

where ε, μ are the permittivity and dynamic viscosity of fluid, respectively, ζ the zeta potential on surfaces, and φ the electric potential.

However, for porous media with pores of varying sizes, the EDL thickness may be comparable to the pore size, and then the structure of EDL is not negligible and even EDLs may overlap, making the Helmholtz-Smoluchowski model invalid. Instead, the ion transport has to be described by the Poisson–Nernst–Planck (PNP) equations in a macroscopic view. Basically, near charged surfaces, the electric potential and ionic concentration fields are intrinsically coupled, described by the electrostatic Poisson equation [1]

$$-\nabla\cdot(\varepsilon\nabla\varphi)=\rho_e=\sum_i z_i e n_i, \tag{2}$$

and the mass balance equation based on the Nernst–Planck formula [1]

$$\frac{\partial n_i}{\partial t}+\nabla\cdot\left(n_i\boldsymbol{u}-D_i\nabla n_i-z_i e b_i n_i\nabla\varphi\right)=r_i, \tag{3}$$

where n_i is the number density of the ith ion species, $\boldsymbol{u}$ the velocity, z_i the valence of the ion (including the sign), e the absolute value of one proton charge, D_i the diffusivity, b_i the ionic mobility, and r_i the source term. Under local electrochemical equilibrium with the source term set to zero, they are typically reduced to the Poisson–Boltzmann (PB) model [4]

$$-\nabla\cdot(\varepsilon\nabla\varphi)=\sum_i z_i e n_{i,\infty}\exp\left[-\frac{z_i e}{k_B T}\left(\varphi-\varphi_\infty\right)\right]. \tag{4}$$

Here, k_B is the Boltzmann constant, T the temperature, $n_{i,\infty}\equiv N_A c_{i,\infty}$ the bulk ionic concentration corresponding to the electric potential φ_∞, and N_A the Avogadro constant. Then, the electroosmotic flow (EOF) is described by incorporating the electric force $\boldsymbol{F}_e=z_i e n_i\boldsymbol{E}$ into the incompressible momentum equation of Newtonian fluid flow [3]

$$\frac{\partial\boldsymbol{u}}{\partial t}+\boldsymbol{u}\cdot\nabla\boldsymbol{u}=-\frac{1}{\rho}\nabla p-\nu\nabla^2\boldsymbol{u}+\boldsymbol{F}_e. \tag{5}$$

For boundary conditions, the non-slip condition $\boldsymbol{u}=0$ is typically applied at solid surfaces, while a given electric potential is set to the zeta potential ζ at nearly the same position as the non-slip velocity boundary.

However, fundamental challenges persist regarding wall confinement effects, and quantitative prediction of electrokinetic transport in saturated porous media remains challenging because of the complicated nonlinear transport within complex pore structures. First, as a continuum-based model, the validity of the PB model becomes questionable within nanoscale confinement where discrete ions and solvent molecular effects emerge, necessitating rigid verification via atomistic simulations [40]. Second, in spite of the continuum assumption being fully satisfied, the complex geometries of porous microstructures and consequent numerous interfaces make the analysis and numerical modeling unacceptably expensive. New tools and new algorithms are urgently needed [41]. Third, hierarchical structures, for example the micro-nano junctions prevalent in membrane systems, exhibit sharp transitions between ion-selective (nanoscale) and electrically neutral (bulk) regions, creating strong non-equilibrium conditions that exceed applicability of the PB model. This requires an examination of traditional Donnan equilibrium theory and current-induced electroconvection mechanisms [42,43]. Last but not least, engineering porous media (e.g. cement paste) introduce spatiotemporal multiscale complexities in ion electrodiffusion – nanoscale Stern layer effects spatially and anisotropic transport temporally – requiring innovative multiscale modeling approaches [44,45].

Therefore, this section discusses very fundamental issues in electrokinetic transport in saturated porous media, focusing on electroosmotic flows (EOFs) and ion transport. The developments of efficient numerical simulations for electrokinetic transport are first introduced, using which the validity of the PB model under nanoscale confinement is first examined, and then the EOF through complex micropore structures is fully modeled and analyzed. Finally, the spatiotemporal multiscale characteristics of electrokinetic ion transport in porous media will be addressed.

2.1. Discrete particle effects in nanoscale confinement

As the system dimension approaches the nanometer scale, the discrete nature of electrical charges and atomic-scale fluid/surface structures becomes significant, driving growing interest in atomistic simulations. Generally, both solvent molecules and ion particles interact with a shifted Lennard-Jones potential [48],

$$V^{LJ}(r_{ij})=4\epsilon_{ij}\left[\left(\frac{\sigma_{ij}}{r_{ij}}\right)^{12}-\left(\frac{\sigma_{ij}}{r_{ij}}\right)^{6}-\left(\frac{\sigma_{ij}}{r_c}\right)^{12}+\left(\frac{\sigma_{ij}}{r_c}\right)^{6}\right], \tag{6}$$

where r_{ij}, ϵ_{ij}, and σ_{ij} are the separation, Lennard-Jones well depth and diameter, respectively, for the pair of atoms i and j. In particular, the interaction is set to zero when molecules are separated farther than a cut-off length $r_c=k_c\sigma$.

In order to approximately describe the interactions between charged particles, electrostatic interactions are calculated using a screened long-range Coulomb potential:

$$V^{C}(r_{ij})=\frac{q_i q_j}{4\pi\varepsilon_0\varepsilon r_{ij}}. \tag{7}$$

where q_i and q_j are the charges of particles i and j, respectively. The vacuum permittivity is ε_0 and there is a uniform dielectric constant ε throughout the simulation cell. A dielectric contrast between solvent and solid could be included, but would require information on the spatial variation of r_{ij} or the use of polarizable potentials [49]. Unlike the Lennard-Jones potential, the Coulomb potential does not have a cutoff because it is known to affect simulations [48]. The long-range Coulomb force makes numerical simulations of large systems extremely expensive. The Ewald summation technique is hugely popular in contemporary molecular dynamics simulation, although it is primarily applied to periodic systems. To reduce computational costs, there are three most popular mesh-based methods for dealing with the potential fluid: Particle-Mesh Ewald (PME) [50], Particle–Particle Particle-Mesh (P^3M) [51], and Fast-Multipole Method (FMM) [52]. To be more efficient, an accurate multigrid particle–particle particle-mesh algorithm has been developed for Coulombic force calculations [53], which has been successfully used to figure out the molecular mechanisms of electrowetting saturation [54], which will be explained in detail in Section 4.

To examine the key discrepancies between MD results and PB predictions in nanochannels – Stern layer effects (sub-nanometer scale), bin size (sampling discretization), and ionic concentration (point-charge assumption validity) – non-equilibrium MD simulations have been conducted for electrolyte solutions confined between planar walls [40,46,49], as shown in Fig. 1 (a–c). There is a scale gap since one has to do statistical averaging of the atomic attributes to obtain the macroscopic variables (density, velocity, pressure, etc.) for transport analysis. In the viewpoint of thermodynamics, those macroscopic variables are meaningful only when the bin size for sampling is sufficiently large, i.e. no smaller than the molecular size [55]. Fig. 2(a–b) presents ion distributions of NaF solution, revealing that when the Stern layer thickness becomes comparable to channel width, the PB theory fails to accurately predict ion distributions across the entire channel, though it remains valid for electric potential in the diffuse layers. The ionic density profiles are demonstrated to match the PB predictions at low-to-moderate bulk concentrations. However, the PB equation becomes inadequate at high bulk concentrations, which is consistent with macroscopic descriptions of its limitations, as shown in Fig. 2(c).

On the other hand, the nanoscale confinement may lead to the EDLs interaction and overlap across the pore, which can also make the PB model fail. To examine the capability of the PB model, the nonlinear solutions of PB model have to be compared with the solutions of the dynamic description of ion transport, i.e. the PNP model, for different cases of EDL overlap. Fig. 2(d) shows that the PB model predicts the net charge density accurately as long as the EDL thickness λ_D is smaller than the channel width W and then overrates the net charge density profile as the EDL thickness increases, and the predicted electric potential profile is still very accurate up to a very strong EDL interaction ($\lambda_D/W\approx 1$) [40].

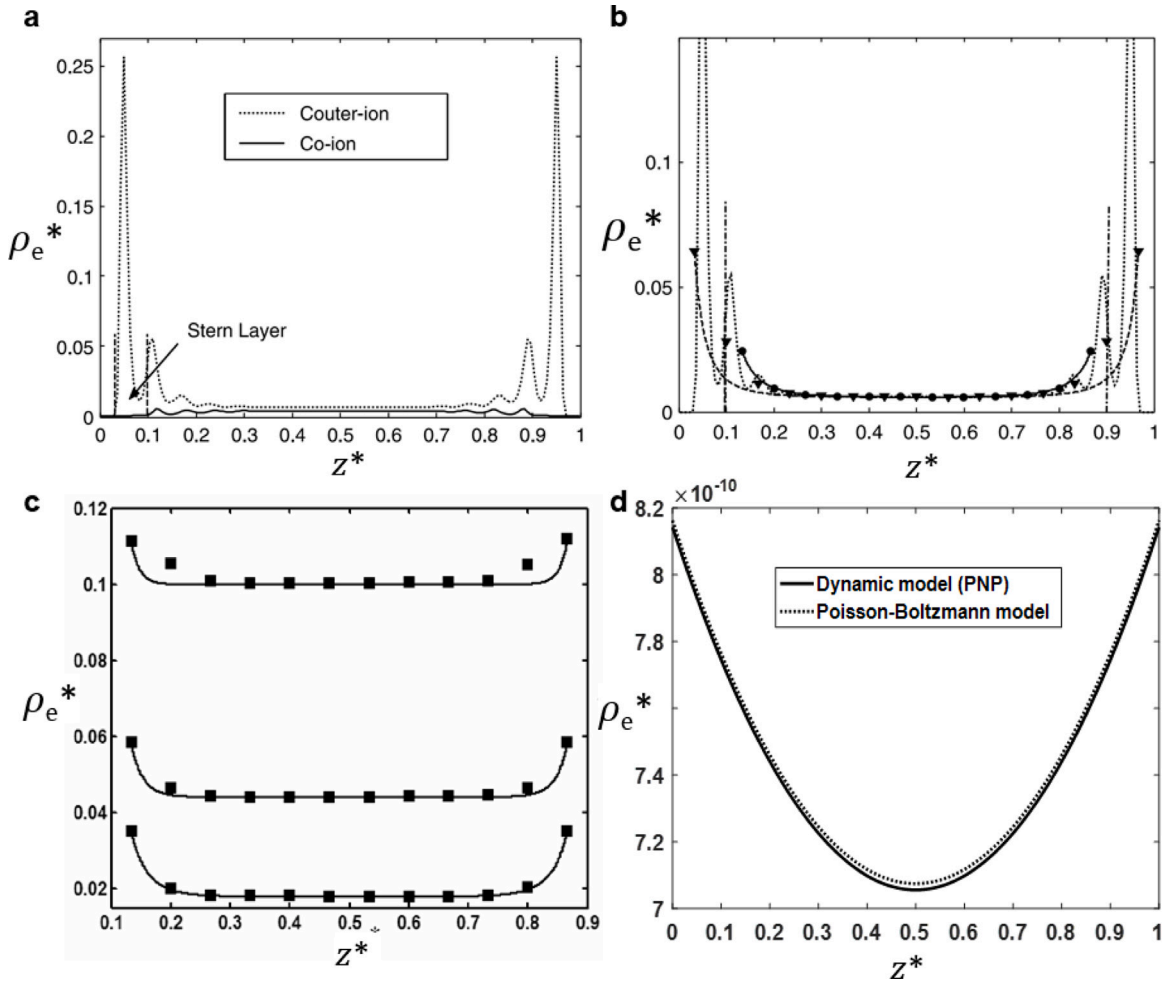

Fig. 2. (a) Stern layer determination from details of MD results [46], and (b) Comparisons between MD simulations and the Poisson–Boltzmann model [46]. Here, the dotted line, circles and triangles refer to the MD results with statistics using different bin sizes, while the dashed line and the solid line are calculated from PB equation with different channel widths and zeta potentials (full channel width or by excluding the Stern layer). (c) Cases of high ionic concentration larger than 1 M. The solid squires are results from MD, while the solid lines are the predictions by the PB model. (d) Net charge density profiles by different models for strong EDL overlapping cases at $\lambda_D/W = 0.92$. The solid line is from the PNP model while the dashed line is from the PB model [40,47]. ρ_e^* denotes the dimensionless net charge density and z^* the dimensionless position across the channel.

2.2. Geometric regulation effects in complex structure

EOF in saturated porous media can be modeled by solving the coupled electrokinetic and hydrodynamic equations, as shown by Eqs. (2)–(5). A non-slip boundary condition for fluid flow and a given zeta potential or surface charge at solid–liquid interfaces make the equations solvable when the dynamic polarization effects at interfaces are negligible [56]. Early studies predominantly employed conventional numerical methods to solve the coupled equations in simple geometries or in its simplified linearized form of PB equations [4,57]. Even though multigrid techniques significantly enhanced the computational efficiency for solving nonlinear PB equations [58,59], they still faced limitations in handling complex geometries [60]. The lattice Boltzmann method (LBM), originating from lattice gas automata, provides a mesoscopic particle-based approach for simulating fluid flow and transport phenomena [61], which was first introduced to electrokinetics around 2000 [62–65]. As a particle-based approach evolving distribution functions on lattices, LBM efficiently handles complex boundaries with simple condition treatments, serving as an effective numerical approach for simulating EOF in complex geometries, first applied to structured charged porous media [66,67].

However, natural porous media typically exhibit random structures, necessitating advanced generation methods. The quartet structure generation set (QSGS) [68], as a part of random generation-growth (RGG) method [41], creates porous structures with statistical properties (including porosity, pore size distribution, grain shape, anisotropy etc.) matching real materials through discrete lattice-based seeding and growth processes, which has been validated by numerous practical cases and experimental data [68–70]. These generated structures integrate naturally with LBM simulations for thermal and static-electrical transport, yielding remarkably accurate predictions of transport properties in complex multiphase materials [41]. Together, RGG and LBM form a powerful toolkit for simulating transport in natural porous materials, sharing lattice structures and locality that enable parallel processing — a milestone in material science [41].

For electrochemical processes and electrokinetic transport, the corresponding LB scheme was proposed in the early 2000s by solving the Poisson equation independently, though the locally electroneutral assumption limited its applicability to charged suspension dynamics [62,63]. Later, a consistent lattice evolution algorithm is developed that couples a lattice scheme for incompressible flows with a lattice solution for electrical potential, called LPBM [65,71]. It inherits the advantages of LBM for efficiently dealing with complex geometries and boundary conditions.

Specifically, the evolution equation of LBM for fluid flow following the method of characteristics is written as

$$f_\alpha(\boldsymbol{r} + \boldsymbol{e}_\alpha \delta_t, t + \delta_t) - f_\alpha(\boldsymbol{r}, t) = -\frac{1}{\tau_v}\left[f_\alpha(\boldsymbol{r}, t) - f_\alpha^{eq}(\boldsymbol{r}, t)\right] + \delta_t F_\alpha, \tag{8}$$

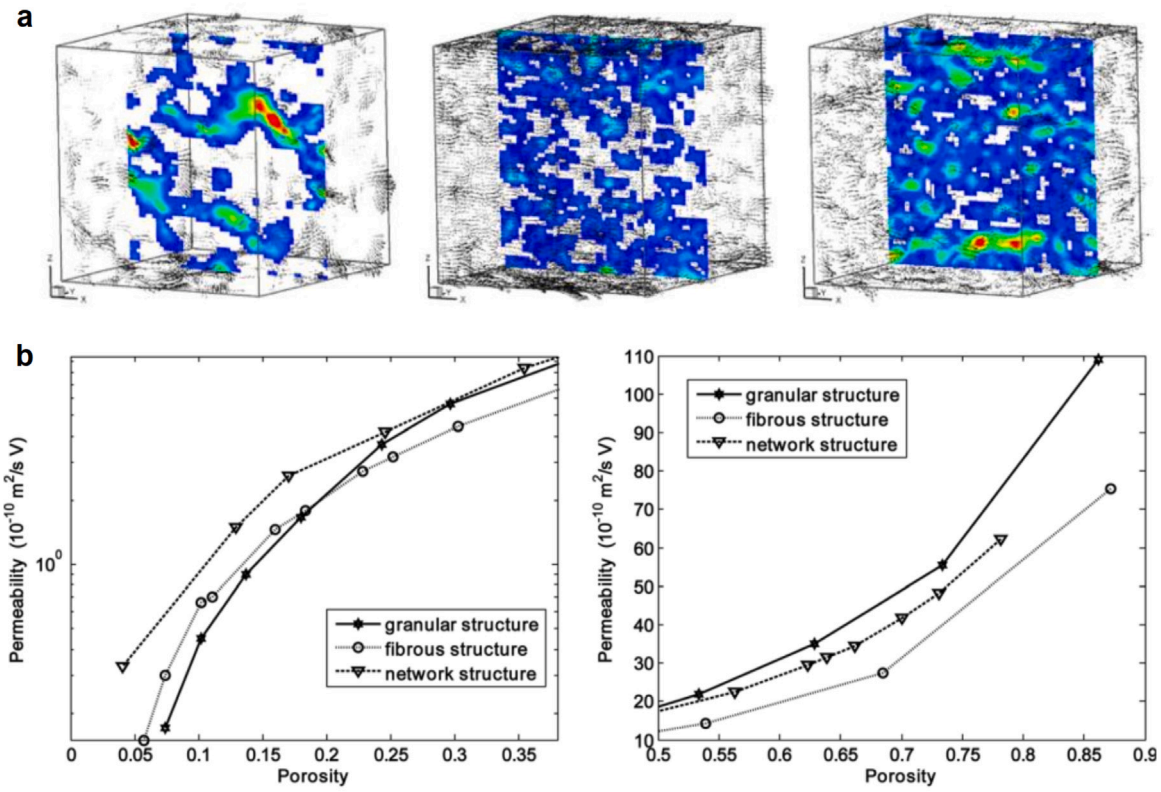

Fig. 3. (a) Velocity fields for different morphology of microstructures of porous media. In particular, the porosity of granular (left), fibrous (middle), and network (right) microstructures is 0.1 [75]. (b) Electro-osmotic permeability as a function of porosity at different porosity ranges: left for the low porosity range (0, 0.38) and right for the high porosity range (0.5, 0.9) [75].

where $\boldsymbol{r}$ is the spatial position vector, $\boldsymbol{e}_\alpha = \sum_k e_{\alpha,k}\delta_k\hat{\boldsymbol{e}}_k$ with δ_k the lattice constant, δ_t the time step, τ_v the dimensionless relaxation time, and F_α the external force density. The macroscopic density and velocity can then be calculated using

$$\rho = \sum_\alpha f_\alpha, \quad \rho\boldsymbol{u} = \sum_\alpha f_\alpha \boldsymbol{e}_\alpha. \tag{9}$$

For numerical modeling of the electric potential distribution under local electrochemical equilibrium, the so-called lattice Poisson method (LPM) extends the original nonlinear Poisson–Boltzmann equation to an unsteady formulation [71],

$$\frac{\partial\varphi}{\partial t} = \nabla^2\varphi + g_{\mathrm{rhs}}(\boldsymbol{r},\varphi,t), \tag{10}$$

with

$$g_{\mathrm{rhs}} = \frac{1}{\varepsilon}\sum_i z_i e n_{i,\infty}\exp\left(-\frac{z_i e}{k_{\mathrm{B}}T}\varphi\right) \tag{11}$$

treating charge density as a source term, which is further discretized through the lattice approach. The LPBM combines LBM and LPM on the same lattice system to ensure consistency. The high efficiency of LPBM for complex geometries and complicated boundary conditions makes it possible for the first time to model electroosmotic flows in natural porous media [69]. This strategy of algorithm developments has been followed for different scenarios [45,60,72–74].

LPBM predictions demonstrate excellent agreements with multigrid solutions across all zeta potentials and with the linearized analytical solution to validate the accuracy [76], and agreements with experimental data for soils for the first time [69]. For $|\zeta| < 30$ mV, the expected deviation from linearized solutions was observed [71]. The LPBM was subsequently applied to investigate microchannel EOF phenomena including surface roughness, cavitation, and heterogeneous charging effects [71,76,77]. A non-monotonic relationship is later revealed between flow rate and roughness spacing, with even sparse roughness configurations reducing flow rates below 90% of smooth-channel values [76]. This underscores the critical importance of accounting for roughness effects in microfluidic EOF analysis. In recent years, it has been shown that when EDL overlapping is considered with a prescribed zeta potential, the linearized P-B equation overestimates the electrical potential from the full P-B equation when the zeta potential magnitude is above V_T, especially for Ca_2^+ ion in solution [78].

As is well known, structural characteristics have crucial effects on electroosmosis, but these effects have never been thoroughly explored due to the great complexity involved. The powerful tool that combines RGG for microstructure reproduction and LPBM for solving governing equations of transports provides the opportunity to make this challenge solvable. Especially, the RGG method can reproduce microstructures with different morphologies within the same framework [41,68,79,80], which means that the morphology effects on EOF can be quantitatively studied for the first time in history. Fig. 3(a) presents the flow fields for three distinct structures (granular, fibrous, and network) at a low porosity of 0.1, revealing that structural effects on electro-osmotic permeability result from two competing mechanisms: the surface-volume ratio (enhancing permeability when increased) and shape resistance (reducing flow velocity). The electroosmotic permeability exhibits markedly different behaviors in two porosity regimes. In the low-porosity regime (0–0.38, Fig. 3(b) left), particularly relevant for geophysical applications, permeability varies dramatically (nearly two orders of magnitude) across this narrow porosity range. Here, network structures demonstrate the highest permeability, while granular structures ($\phi < 0.15$) or fibrous structures ($\phi > 0.2$) show the lowest values. This structural effect becomes particularly pronounced at very low porosities ($\phi < 0.1$). Conversely, in the high-porosity regime (0.5–0.9, Fig. 3(b) right), important for energy systems, granular structures consistently outperform others in permeability. Fibrous structures exhibit the lowest permeability throughout this regime, reaching only about half that of granular structures at equivalent porosity [75].

For industrial applications, two more important factors have to be examined: the non-Newtonian behavior of electrolyte solutions [81] and the permittivity effect of the solid phase, which can be primarily explored by adopting the extended LPBM tools. The non-Newtonian effect, related to shear-thinning/thickening behavior, can be described by a power-law model with flow behavior index n [82,83]. Electro-osmotic permeability is demonstrated to decrease with increasing n, with this effect being most significant in granular structures. The permittivity effect, characterized by the dielectric constant ratio $\varepsilon_r \equiv \varepsilon_s/\varepsilon_l$ [84], shows that the permeability decreases with the permittivity of the solid phase. Constant electric field assumptions yield underestimated permeability values, while treating the solid as ideal dielectric (with assumed zero permittivity) leads to overestimation. The lattice methods have also been applied to study electrokinetic transport near ion-selective surfaces and in flow batteries [85–91].

Ion-selective membranes are widely used in various applications, such as fuel cells, batteries, and water desalination. To uncover the effect of detailed nano-structures, additional molecular insights of membrane functions have been provided through the simplified porous structure, such as microchannel and nanochannel interfaces [7,92]. On the one hand, the Donnan equilibrium $c_L = Dc_R$, though widely used in nanofluidic systems to determine ionic concentrations and electrical potentials at channel-reservoir interfaces, originates from classical thermodynamic theories with equilibrium assumptions [93,94]. It is demonstrated that the applicability of the Donnan equilibrium model becomes questionable under strongly non-equilibrium transport conditions at nanochannel-reservoir interfaces [42]. By numerically solving the Poisson–Nernst–Planck model for ion transport, the exact distributions of ionic concentration and electrical potential are obtained, enabling quantitative comparison with Donnan equilibrium predictions. Systematic variation of channel length, reservoir ionic concentration, surface charge density and channel height reveals the Donnan equilibrium's limitations for short nanochannels, large concentration differences and wide openings. To quantify the non-equilibrium effects, a dimensionless Q factor is introduced, defined as $Q = (f_{i,\mathrm{in}}/f_{i,\mathrm{L-bulk}})\exp\left((\mu_{i,\mathrm{in}} - \mu_{i,\mathrm{L-bulk}})/k_BT\right)$, whose relationship with operational conditions $\theta = (\Delta c/c^*)(H/L)^{1/2}(\lambda_D/L)$ is thoroughly examined. On the other hand, electroconvective flow near ion-selective surfaces drives ion and water movement [95–100], yet the origin of the small cation population in the extended space charge (ESC) region remains unclear. This phenomenon has been investigated using a blockage-nanoslot-bulk structure, solving the coupled Poisson–Nernst–Planck and Navier–Stokes equations [43]. The transient analysis of local fluid dynamics, voltage, and charge distribution identified ion-flux-induced strong electric fields as crucial for ESC formation. When the limiting current density is exceeded, the resulting negative field drives a parallel cation extension at the nanoslot-bulk interface, creating the ESC's characteristic localized charge peak. The study quantified the self-similar expansion of ESCs through thickness variations and revealed normalized charge density structures using scaled coordinates validated by simulations. Furthermore, geometric effects on vortex patterns demonstrated the role of nanoslots in enhancing the accuracy of wave-number prediction.

2.3. Spatio-temporal multiscale effects

Clay/cement materials are widely encountered in the transport of heavy ions in soil treatments, groundwater contamination, nuclear waste disposal, and anticorrosion of marine structures, where understanding of the ion transport mechanisms through cementitious materials is of great importance for predicting their long-term performance and service life. The dominant pore space can be distinguished using the concept of capillary pore percolation. When the capillary porosity depercolates, the gel pores in the calcium-silicate-hydrate (C-S-H) phase form the dominant pathway for transport in cement paste. At this stage, the nano-scale effects on ion transport would play an important role [101,102].

Understanding cation transport mechanisms through barrier materials is crucial for energy and environmental applications. Studies show that at low concentrations, cations diffuse through compacted clay faster than neutral or anionic species, primarily due to electrostatic interactions with negatively charged clay surfaces. This enhanced transport, known as surface diffusion, occurs within the electric double layer, including the diffuse layer $\boldsymbol{j}_i^{**} = -D_{i,0}\nabla n_i - z_i e b_{i,0} n_i \nabla\varphi$ and the solid surface $j_{i,s}^{**} = -D_{i,s}\partial n_{i,s}/\partial s$, where $D_{i,0}$ and $b_{i,0} = D_{i,0}/k_BT$ are the diffusion coefficient and ionic mobility of the ith ion species in the free water, and $D_{i,s}$ is the surface diffusivity. Pore-scale simulations were employed to examine electrokinetic effects on cationic tracer diffusion [104], revealing that the normalized volume charge density significantly influences cation diffusion. Notably, electrokinetic effects on chloride transport become negligible when the dimensionless Debye length (defined as the ratio of maximum-probability pore size to the Debye length) exceeds 32 in cement-based microstructures. For practical applications, a predictive formula is developed by pore-scale modeling to correlate effective chloride diffusivity with electrokinetic effects in cement paste [105]

$$D_{\mathrm{eff}} = D_0\left[\exp\left(-0.45be^{-0.17l^*/2}\right)\cdot\phi_{\mathrm{cap}}\right]^{1.7}, \tag{12}$$

where D_{eff} and D_0 represent the effective and the bulk diffusivity, respectively; $\zeta_i^* = z_i e\zeta/k_BT$ is the dimensionless zeta potential, $l^* = d/\lambda_D$ the dimensionless pore size with d denoting the characteristic pore size and λ_D the Debye length, and ϕ_{cap} the capillary porosity. These simulation methods can be extended to study ion transport in unsaturated or cracked cementitious materials, where water films or cracks serve as transport pathways [106–113].

Experimental studies reveal that chloride ion diffusivity in concrete structures closely matches tritiated water (HTO) while exceeding sodium ion mobility, a phenomenon attributed to electrical double layer (EDL) effects near charged C-S-H surfaces [114,115]. To elucidate transport mechanisms in C-S-H and quantify effective diffusivities, a multiscale modeling approach is developed integrating atomic- and pore-scale simulations [44,116] (Fig. 4(a)). The pore-scale model employs the lattice Boltzmann method to solve modified Nernst–Planck equations incorporating steric effects and ion-ion correlations through excess chemical potential corrections μ_i^{ex} derived from grand canonical Monte Carlo atomic-scale calculations, i.e.

$$\boldsymbol{j}_i^{**} - n_i\boldsymbol{u} = -D_{i,0}\nabla n_i - z_i e b_{i,0} n_i\nabla\varphi - n_i\frac{D_{i,0}}{k_BT}\nabla\mu_i^{\mathrm{ex}}. \tag{13}$$

Here, the excess chemical potential in the Stern layer along the direction perpendicular to the solid surface is given by

$$\mu_i^{\mathrm{ex}}(x) = -ez_i\psi^{\mathrm{GCMC}}(x) - k_BT\ln\left(\frac{n_i^{\mathrm{GCMC}}(x)}{n_{i,\infty}}\right), \tag{14}$$

where x is the perpendicular distance to the solid surface. This multiscale analysis demonstrates significant Stern-layer contributions to ion transport in pores below 10 nm diameter and successfully reproduces experimental diffusivity trends for various ions. The methodology proves equally applicable to analyzing EDL-influenced transport in proton exchange membrane fuel cell gas diffusion layers [117].

Accurately predicting long-term ion diffusion behavior incorporating pore-scale EDL effects remains a significant challenge, as characteristic diffusion timescales in representative elementary volumes (REVs) typically measure microseconds — ten orders of magnitude shorter than required timespans. A numerical upscaling scheme for ion diffusion in charged porous media with EDL effects is developed [45] (as shown in Fig. 4(b)). Through scaling analysis of dimensionless pore-scale transport equations, they identified conditions for decoupling electrical and diffusive effects, establishing appropriate temporal and spatial scales for surface diffusion through EDL. The lattice Boltzmann-based

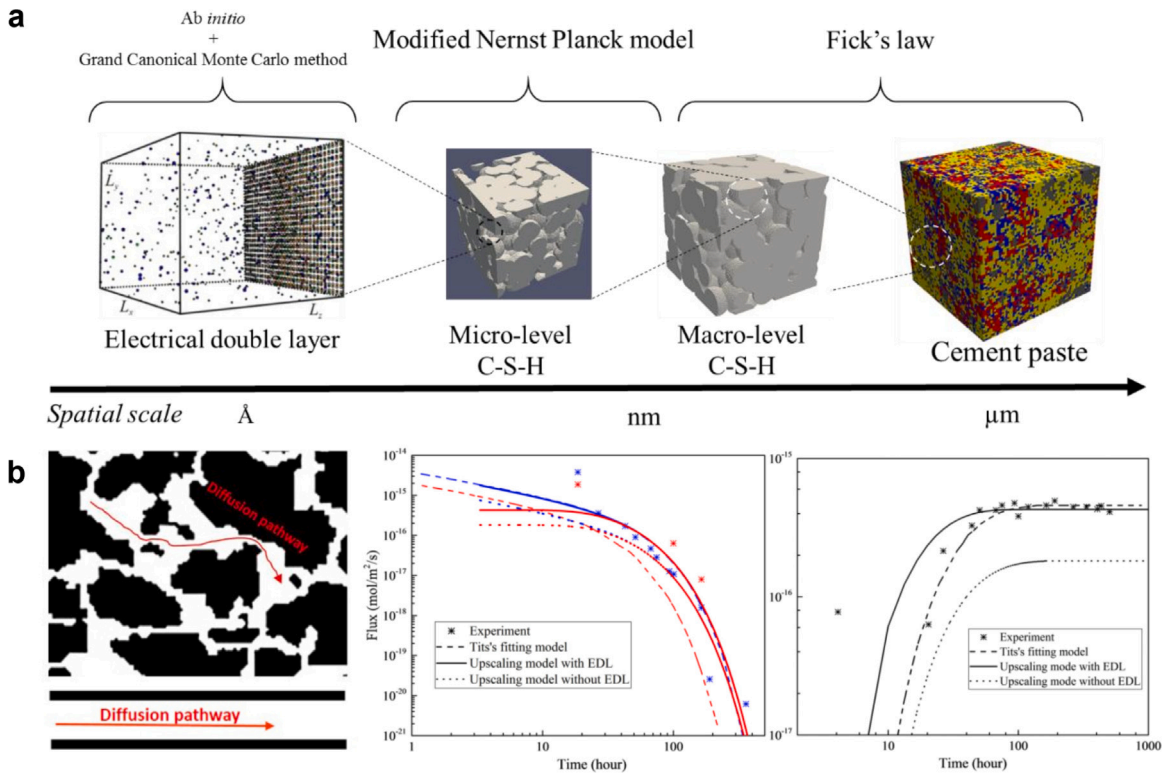

Fig. 4. (a) Hierarchical representation of the cement paste structures and the multiscale modeling approaches [44]. (b) The sketch of scale reduction based on the tortuosity of the diffusion pathway (left), and the comparisons between the upscaling model, the fitting model and the experiment data from literature [103] for through-diffusion (middle) and out-diffusion (right) [45].

upscaling scheme demonstrates excellent agreement with full-scale simulations for both steady- and unsteady-state surface diffusion in straight channels, accurately reproducing electrical potential and concentration profiles. The method successfully predicts tracer-ion through-diffusion and out-diffusion in hardened cement pastes, matching both full-scale simulations and experimental data without parameter fitting. This approach effectively bridges ion diffusion behaviors across time scales, advancing the understanding of long-term transport mechanisms in charged porous media [45]. This multiscale framework can be extended to investigate ion transport in slits or fractures [118,119], and the multiscale EK effects due to multiple temporal scales in oscillatory flow through porous media are also explored [120,121].

3. Electrokinetic transport in saturated porous media: effect of field inhomogeneity

In the last section, the zeta potential, or the surface charge density equivalently, is given uniformly at a constant value as the boundary condition for the electrical potential (Poisson) equation. In fact, the local zeta potential or surface charge may vary with local properties of solid surface and liquid [6], such as temperature, ionic concentration, and pH value. However, for simplicity, the zeta potential of a system can have an effective value by matching the predictions and experimental data, which is how the zeta potential is determined in practice [1], even though the local zeta potential on the surfaces can vary somehow. This approximation has been working well for predictions of electrokinetic transport in a "mild" environment, where the environmental factors, such as concentrations, temperature, and so on, vary negligibly or slightly. Large amounts of examples can be found in the last century [56,58] and in some cases in the past twenty years [69].

However, as we know that the solid–liquid interface achieves surface charge by surface reaction of ions, the so-called surface complexation on the solid side or charge regulation on the liquid side, which actually is strongly dependent of the environmental factors [122–124]. Therefore, the homogeneity assumption of zeta potential or surface charge density on surfaces will be broken by significant variations of (i) properties (concentration, pH, ionic type) of liquid solution, (ii) properties of solid surfaces, and (iii) temperature of solid and liquid. These cases are not rare in nature and engineering applications, but have been rarely reported because of complexity and difficulties in the study. In fact, the field-induced gradient of the surface charge density, which is not directly accessible on the nanometer scale and usually assumes a prescribed distribution, is the key to account for the steady-state current–voltage curve from experimental measurements in a single conical glass nanopore [125]. In addition, time-dependent functions such as negative differential resistance and hysteresis are unique electrokinetic properties emerging in nanoscale conical pores, which also addresses the effects of local geometric variation on electrochemical and mechanical behaviors in porous media [126,127]. Rational prediction of charge regulation effects requires knowledge from multiple disciplines (physical chemistry, mechanics, transport theory, thermodynamics, etc.), technologies and views from multiscale and multiphysics. It is also noteworthy to address the difficulty of measuring zeta potential in minerals, leaving a gap between the predictions and experiments. In fact, the reported values in the literature are highly variable, often showing inconsistent or even contradictory trends. Nevertheless, this is often the case for complex systems with multiphysical and multiscale features, which makes accurate modeling vital for further experimental validations.

In this section, the electrokinetic transport in inhomogenously charged porous media will be first introduced considering the charge regulation triggered by ionic concentration or pH inhomogeneity. The reactive transport in porous media will then be briefly discussed by considering the ionic homogeneous or heterogeneous chemical reactions in solution. Finally, we will address the temperature effects on either the surface charge regulation or the ionic thermodiffusion transport in saturated porous media.

3.1. Concentration effects via charge regulation

It is well known that the surface charge density at a solid–liquid interface is not constant but varies with the local properties of both solid and liquid [1]. Experiments indicated that surface charge density is a function of the local concentrations of metal ions and proton, based on which an electrical triple layer (ETL) model [12,128,129] has been established by considering the surface complexation reactions between ions in electrolyte solution and surface siloxane groups and adding this reaction layer to the classical electrical double layer (EDL) model [1]. Based on the ETL model, the surface charge density or zeta potential can be quantitatively determined depending on the local properties of solid and electrolyte solution, such as the ionic concentration and pH etc.

Fig. 5(a) sketches a typical electrokinetic structure of the silica surface based on the ETL model [12,128]. In the pH range 3–9, the typical chemical reactions at the silica surface can be written as

$$\mathrm{SiOH_2^+} \rightleftharpoons \mathrm{SiOH} + \mathrm{H^+}, \quad (K_1) \tag{15}$$

$$\mathrm{SiOH} \rightleftharpoons \mathrm{SiO^-} + \mathrm{H^+}, \quad (K_2) \tag{16}$$

$$\mathrm{SiO^-} + \mathrm{M^+} \rightleftharpoons \mathrm{SiOM}, \quad (K_M) \tag{17}$$

$$\mathrm{SiOH_2^+} + \mathrm{A^-} \rightleftharpoons \mathrm{SiOH_2A}, \quad (K_A) \tag{18}$$

where K_i's are the associated equilibrium constants for the reactions, respectively. More reaction equations can be easily added for multi-component electrolyte and for multi-valent cations [12]. Therefore, this model is not limited to the binary salt. The silanol group may become positively charged by accepting protons under very acidic solutions (pH < 3), and the silica significantly dissolves into silicate ions in basic solution (pH > 9); therefore, this model has to be modified beyond the pH range 3–9 [130]. Note that in Fig. 5(a) the adsorption of anion A^- by the $SiOH_2^+$ sites is sketched by a dashed-line connection because this reaction rate is extremely low at the pH range 3–9. Sometimes, this full triple-layer model with over ten equations are coupled is too complex to use. People proposed a simplified version, that is, the basic Stern model [131], to calculate the surface charge or the zeta potential just by coupling two equations. The basic Stern model is very popular and easy to use [5,132–135], however, with the cost of losing accuracy for higher salinities compared to the triple layer model and experimental data [136,137], as shown in Fig. 5(a). Indeed, the "macroscopic" Helmholtz-Smoluchowski approach with the classical EDL model and no Stern layer contribution has been used for more than a century, but it is clear that this model cannot be used when surface conductivity is too important [138] or in partially saturated conditions [139]. The effective excess charge approach with the ETL model, first proposed by Kormiltsev and then developed by Revil and Leroy [140,141], can be found in detail in a recent paper [121].

The mechanism of electrochemical charge regulation in equilibrium was initially studied for isolated charged surfaces, and the triple layer model has worked pretty well since proposed in the 1970s [12,128,129] until the early 2010s when some experimental data was reported for ion transport in pores of a few nanometers which could not be explained by the existing theories [142]. For the electrokinetic transport in nanoscale pores, there are three novel important features compared with those in large-scale pores: (i) the electrical diffuse layer may often interact with each other resulting in the EDL overlapping which could further impact the charge regulation, (ii) the salt concentration is usually high where the Stern layer is not negligible and the effective charge density is changed [143], and (ii) the position of zeta potential plane (also called the *slipping plane*) within the diffuse layer may not coincide with the outer Helmholtz plane [144], which will influence the fluid flow behavior at nanoscale.

Charge regulation from double-layer overlap in confined spaces decreases the surface charge density but increases the zeta potential on silica surfaces [145]. The truncation of Gouy–Chapman diffuse part in compacted clay-rocks and bentonite was introduced into the electrical triple-layer model, which was able to capture the variation of the osmotic efficiency and the swelling pressure with the given mean pore size. The partition of counterions between the Stern layer and the diffuse layer as a function of the pore size calculated by the TLM also showed good consistency with the model, implying that more than 90% of the counterions were located in the Stern layer [146]. Once the specific adsorption of anion is not negligible, the four-layer model may be more suitable to describe the ions distributions because of the size difference between cations and anions [147], where a concentration-dependent (flow-)inactive buffer layer is incorporated [148] (as shown in Fig. 5(b)). Thermodynamic analysis validated the buffer layer's thickness variations, with predicted ionic conductances matching experimental data in nanochannels [148]. The model reveals that the buffer layer thickness saturates to a minimum in concentrated solutions, providing critical insights for designed ion transport in nanosystems.

To this end, the theoretical models shown in Fig. 5 tell us that the surface charge at solid–liquid interfaces is really a function of the local electrolyte properties instead of assumed a uniform one in the previous studies. These models also enable us to capture the local surface charge density during the coupled transport process. However, once EDLs are overlapped in nanochannels, when considered the electrokinetic transport within asymmetric structures or under external fields, even if the electrochemical equilibrium (with the PB equation held) may be assumed in the transverse direction along the boundary point-by-point, the full-coupled resolution of inhomogeneous electrochemical boundary is still hard to obtain. In fact, the difficulty and challenge come from the real coupling of three factors: local property variation during flow, local surface charge and local property change by EDL overlap. Therefore, some effective models have to be proposed to solve the inhomogeneous charge regulation in the presence of EDL overlapping [135,151]. The hierarchical pore size feature of natural porous media makes this difficulty even tougher. To make this problem easier, a classification of electroosmosis has been proposed based on a dimensionless number $M = \lambda_D/d$, representing the ratio of Debye length to pore size d [135].

For $M < 0.01$ (thin EDL limit), EOF velocity with charge regulation boundaries can be directly determined, as seen in microchannels and around inhomogeneously charged spheres [152,153]. The semi-analytical charge regulation model captures experimental hysteresis without fitting parameters and classifies proton transport into pH-dependent shock/rarefaction/discontinuity regimes [152]. The numerical framework that combines LPBM with RGG-generated 3D porous media is employed to study charge regulation effects on EOF under varying conditions [154]. Permeability grows exponentially with surface potential above about 50 mV, and increases with ionic concentration despite decreasing zeta potential, contradicting thin-layer models. In a four-ion systems (Na^+, Cl^-, H^+, OH^-), nonlinear velocity responses and reverse flows in reconstructed media is revealed using LBM (Fig. 6(a)), which is consistent with the experimental data [155] in soil processing and reflects the essential role of pH- or concentration-modified surface charge in EOF within porous media [135]. In the non-overlap regime at $0.01 < M < 0.1$, the modification factor Θ similar to the slip modification for gas flow at $0.01 < \mathrm{Kn} < 0.1$ can be defined to the EOF velocity

$$\Theta \equiv \frac{u_{\mathrm{avg}}}{u_{\mathrm{HS}}} = 1 - \frac{8M}{\zeta^*} \tanh\left(\frac{\zeta^*}{4}\right). \tag{19}$$

Here, $\zeta^* = e\zeta/k_BT$ is the dimensionless zeta potential, u_{avg} is the average velocity of EOF, and u_{HS} is the velocity predicted by the Helmholtz-Smoluchowski (HS) equation. The modification shows good performance within a large range of ζ^* and M [156–158].

For the electroostic flows in nanopores where EDL overlapping is significant (commonly in ion-selective membranes), the entire pore lacks an electroneutral region, corresponding to partially-overlapped

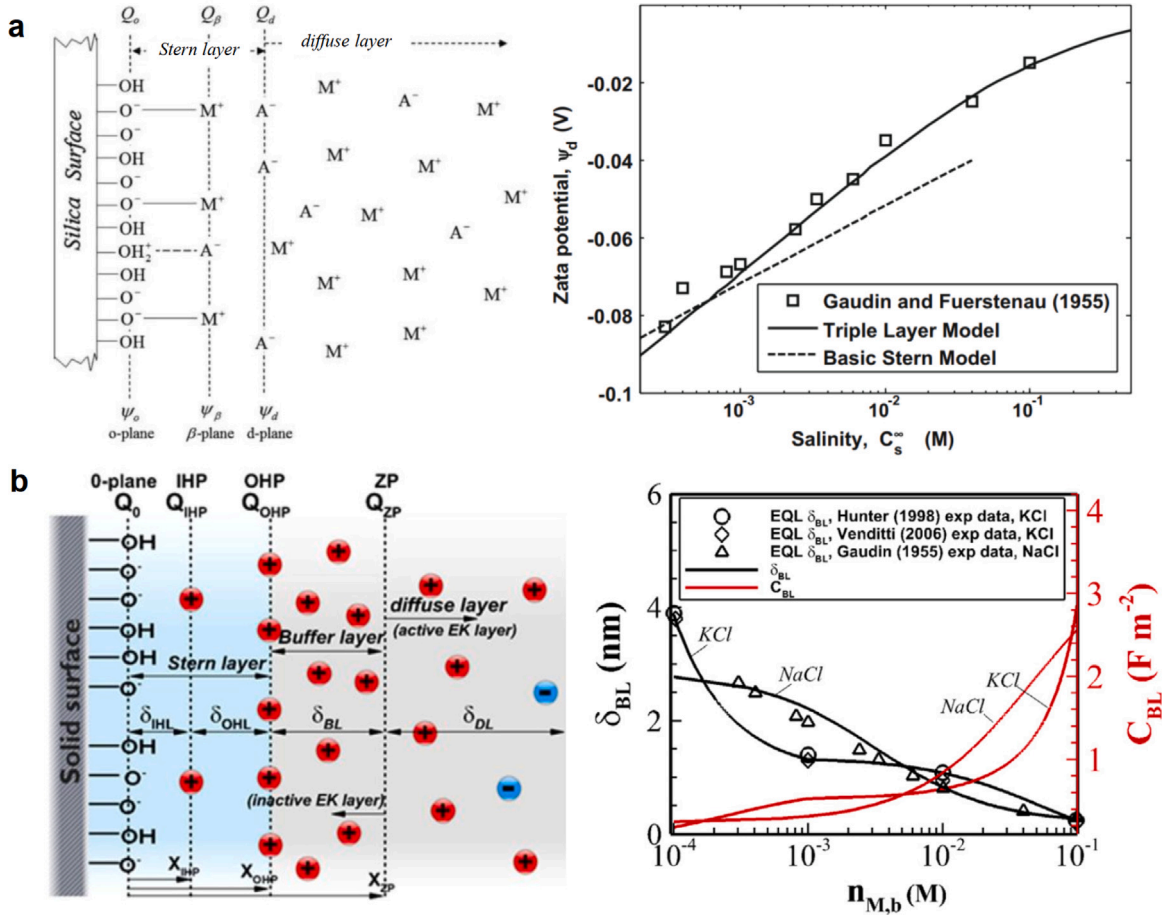

Fig. 5. (a) Schematics of the electrical triple layer (ETL) model and the salinity effect on the surface charge density [145] compared to the experimental data [136] (b) Schematics of the electric quad layer model by introducing a buffer layer based on thermodynamic analysis into ETL (left) [148,149] and the best-fitted δ_{BL} (right) for KCl solution [148] by the previous experimental data [1,137,150].

($0.1 < M < 1$) and fully-overlapped ($M > 1$) regimes. In fully-overlapped cases, the transverse direction becomes essentially equipotential. Reverse electrodialysis exemplifies energy conversion from salinity gradients, where streamwise concentration variations induce changing surface charge densities. The Basic-Stern model is adapted to relate the surface charge density with the local concentration, improving predictions of current–voltage curves and electromotive forces [159]. Their modification replaces hard-to-measure surface charge densities with accessible parameters, achieving better agreements with experimental data than the previous models. For partially-overlapped regimes, especially in porous media with wide pore size distributions, comprehensive models predicting local surface charge densities from solution properties remain scarce. Fig. 6(b) shows the representative-bulk layer model [160] for estimating local effective concentrations in overlapping EDLs, later applied to nanoporous rocks [161–167]. However, several factors need to be further studied in the future. On the one hand, the thickness of the representative-bulk layer, the effective ionic concentration, and the reference potential need to be verified, particularly for consistency with established models in uniform nanochannels. On the other hand, the assumed transverse electrochemical equilibrium may fail when the surface conduction of the Stern layer becomes significant under applied electric fields [168].

3.2. Concentration effects via kinetic transport

When reactive transport or adsorption dynamics at surface is involved, not only the solid structure may change through dissolution or precipitation, but also the normal ionic flux will be non-zero, which will further interact with electrokinetic transport (such as fluid convection, diffusioosmosis, electroosmosis, *etc.*) in porous media.

Carbon capture and storage (CCS) is a pivotal technology for mitigating climate change. To understand the underlying pore-scale mechanisms, the CO_2-saturated fluid injection in limestone at pore scale is investigated using LBM [169]. The pore structure was reconstructed from digitized limestone thin sections, with simulations performed for varying mineral reaction rates (Fig. 7(a)). In particular, the heterogeneous reactions between aqueous species and minerals at the pore-mineral interface are given by

$$AD\frac{\partial \varphi}{\partial n} = \sum_s \nu_{js} A_s I_s, \tag{20}$$

where A is the total surface area, A_s the individual mineral surface area, D the aqueous diffusivity, and I_s the reaction flux of the sth mineral across its surface, taken as positive for precipitation and negative for dissolution. Results demonstrate that decreasing reaction rate constants lead to more uniform dolomite deposition around dissolving calcite grains. Eventually, pore blockage occurs when major flow channels become obstructed, terminating fluid transport. The negative reaction rate for calcite versus positive rates for dolomite and gypsum quantitatively confirms concurrent calcite dissolution with dolomite/gypsum precipitation.

The coupled electrokinetic and reactive transport in micropores is investigated through mesoscopic modeling [74], as illustrated in Fig. 7(b). A numerical framework integrating multiple LB models is developed to simultaneously account for ion transport mechanisms and their influence on heterogeneous reactions in micropores. To describe

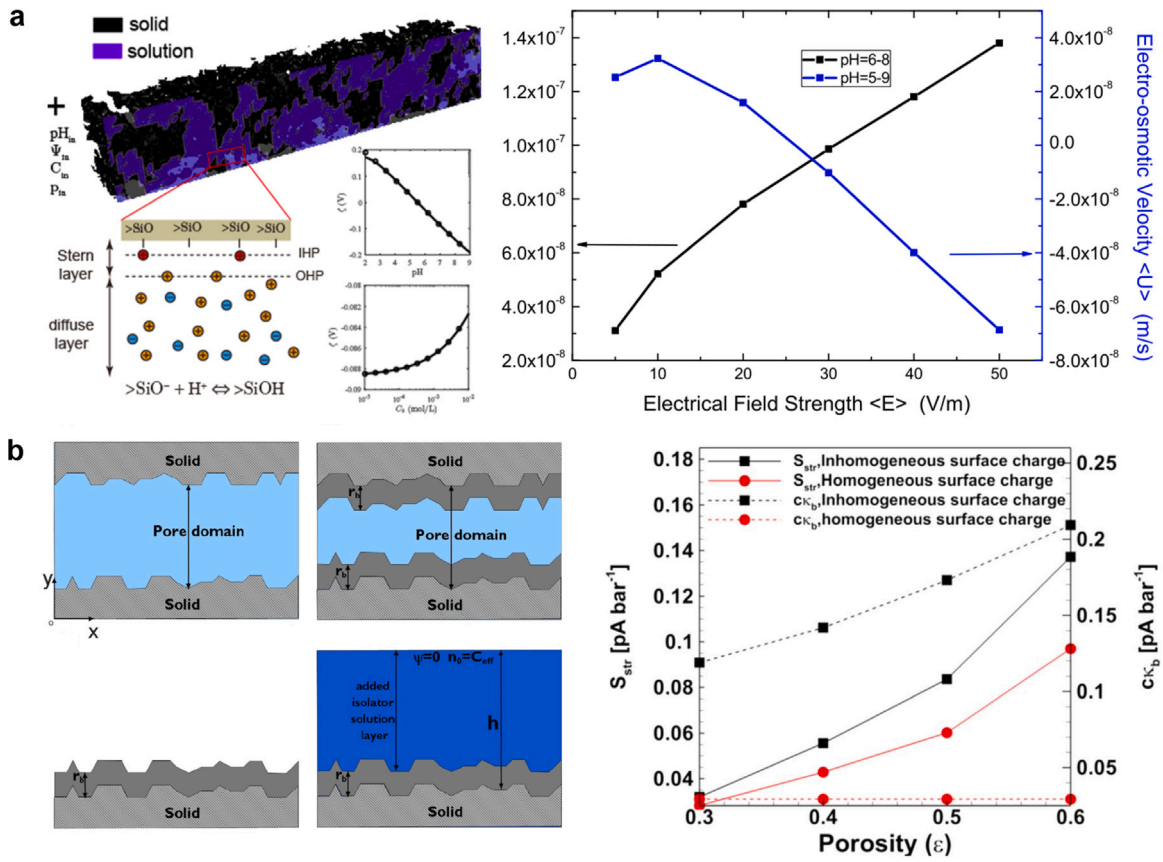

Fig. 6. (a) The simulated electroosmotic flow in inhomogeneously charged porous media by considering the local charge regulations in the pores. The 3D granular porous microstructure was generated by QSGS [68] and the governing equations were solved by LPBM [76]. The simulations reproduced the reverse flow in electroosmosis for the first time, which has been reported by experimental data for a long time [155]. The mechanism lies in accumulation of hydrogen ions by the inhomogeneous surface charge and significant change of pH distribution along the flow direction [135]. (b) When EDLs overlap in pores, a representative-bulk layer model (left) was proposed to find out the local effective bulk concentration [160], and the predictions (right) of streaming conductance S_{str} and the coupling factor times bulk solution conductivity $c\kappa_b$ in nanoporous media [161].

the reaction kinetics, the heterogeneous reaction is described by the transition state theory

$$I_{\text{heter}} = -k_r(1 - K_{\text{eq}}Q_0), \tag{21}$$

where k_r and K_{eq} are the reaction rate constant and equilibrium constant, respectively. Q_0 is the ion activity product defined by

$$Q_0 = \prod_i \left(\gamma_i c_i^s\right)^{\alpha_i}, \tag{22}$$

where γ_i is the activity coefficient, c_i^s the ionic concentration on the surface, and α_i the stoichiometric coefficient of reactions for the ith ion. The study examines the role of surface charge in reactive transport for an ion precipitation scenario, revealing a competition between transport and reaction governed by their characteristic rates, characterized by the second Damkohler number $\text{Da} = k_r h/c_\infty D$. When transport processes (diffusion and convection) are significantly slower than reactions (transport-dominated regime), surface charge substantially inhibits the reaction. In contrast, in reaction-dominated cases, surface charge effects become negligible. This modeling approach has been further applied to investigate reactive transport, capacitive deionization, and electrokinetic remediation in multiscale porous media [172–177].

If the pore structure can be represented by an ensemble of capillary tubes, under the hypothesis of a uniform dissolution or precipitation of the pores, the electrokinetic properties of porous media can be predicted by an analytical model [178]. Recently, the dispersion of a charged solute in charged micro- and nanochannels with reversible sorption is investigated, deriving analytical solutions for the mass fraction in the fluid, transport velocity, and dispersion coefficient [170], as illustrated in Fig. 7(c). The electric double layer (EDL) formed on the charged surface modifies the transverse distribution of solute, leading to charge-dependent transport. In particular, the law of mass action for reversible sorption and mass balance of the solute on the interface give

$$K_d = \frac{s}{c}, \quad \frac{\partial s}{\partial t} = -D\frac{\partial c}{\partial n} - zebc\frac{\partial \varphi}{\partial n}, \tag{23}$$

where K_d is the apparent equilibrium constant of sorption, s and c the sorbed surface solute and solved bulk solute concentration, and n the normal vector pointing outwards the surface. The analysis reveals that the interplay between sorption and the EDL introduces charge-dependent effects even for thin double layers. However, by incorporating the intrinsic sorption equilibrium constant, this complex behavior can be simplified to a non-charge-dependent scenario.

3.3. Temperature effects and multi-physical transport

Temperature gradient is another important factor that can affect the surface charge density and the ionic transport in porous media, which can be induced by external heating or cooling, or by the Joule heating due to the applied electric field. The temperature variation can not only give rise to the diffuse layer thickness modification and inhomogeneous surface charging, but also cause thermodiffusion, which is the migration of ions due to the temperature gradient. The thermodiffusion effect can enhance or suppress the ionic transport depending on the sign of the temperature gradient and the type of ions [179,180]. In addition, under axisymmetric thermal loadings, the temperature gradient can also induce the thermo-osmosis effect [181–183].

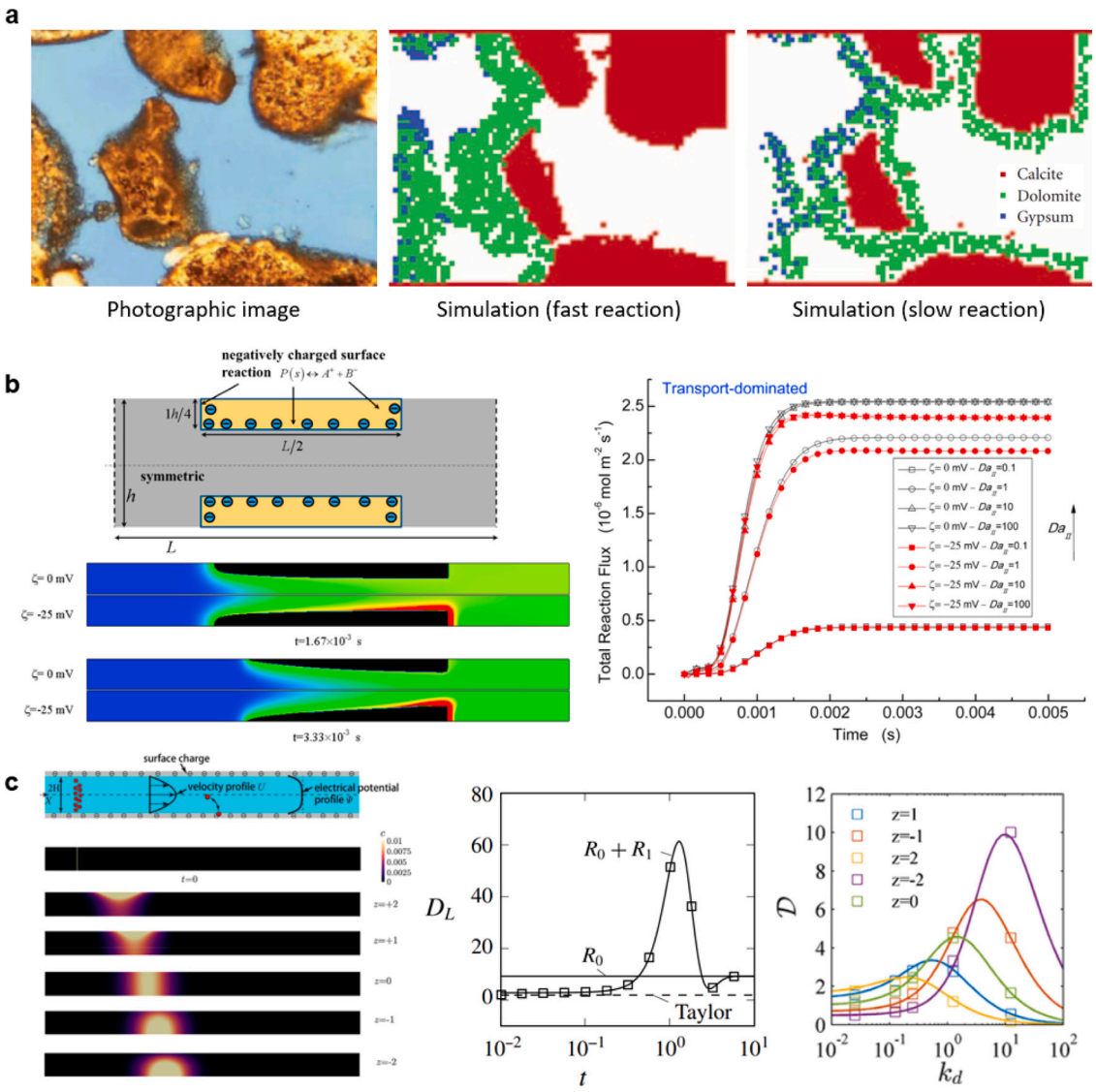

Fig. 7. (a) Photographic image of a limestone rock thin section (left) and the LB simulation results geometries (right) for two different mineral reaction rate constants [169]. (b) Distribution of counterion concentration (left) and total reaction flux evolution (right) in 2-D dissolution [74]. $Da \equiv k_r h/c_\infty D$ denotes the Damkohler number. (c) Schematics and simulation results of dispersion of charged solute in charged microchannel with reversible surface sorption at dimensionless times $t = 0$ and $t = 50$ (left) [170]. Analytical solutions of evolution of dispersion coefficients (D_L, $\mathcal{D}$) for neutral solute transport (middle) and charged solute transport (right) with sorption in Poiseuille flow are compared between the classical theories and numerical results [170,171].

Mixing remains challenging in microchannels due to low Reynolds number conditions. A vortex-based mixing enhancement method for electro-osmotic flows is proposed using temperature-patterned walls [72]. For the non-isothermal fluid, the standard Nernst–Planck equation was modified by adding a temperature-dependent migration term involving both thermal and electric potential gradients. Simulation results demonstrate that the asymmetric wall arrangement is the most efficient configuration, improving mixing performance by 39% at Reynolds numbers of 10^{-3}. When temperature gradients are applied at both walls and inlets, the resulting thermal differences generate entrance-region vortices that further enhance mixing [73]. Here, the thermodiffusion effect is also included in the ion transport equation

$$\frac{\partial n_i}{\partial t} + \boldsymbol{u}\cdot\nabla n_i = D_i\nabla^2 n_i + \frac{z_i e D_i}{k_B}\nabla\cdot\left(\frac{n_i}{T}\nabla\varphi\right), \tag{24}$$

where T denotes the temperature field. This approach enables precise vortex scale control without additional components, offering unique advantages for active mixing regulation in electro-osmotic microflows.

Recent years have witnessed diverse ionic current rectification methods for nanofluidic chips [187–190]. It is theoretically demonstrated that temperature gradients can effectively manipulate ionic rectification in tapered nanochannels when applied either from tip-to-base or base-to-tip directions [184], as illustrated in Fig. 8(b). Through the assumed decomposition of the electric field into the internal and applied ones, their results show that base-to-tip temperature gradients significantly enhance the rectification ratio, while reverse gradients suppress it. This rectification behavior depends primarily on the electrical double layer overlap regime at the nanochannel tip. The authors developed a semi-analytical solution capable of reproducing numerical results with comparable magnitude. It is noteworthy that the above decomposition assumption still requires further verifications, since the concentration polarization phenomenon in the tapered nanochannels may not be negligible, which may trigger the complex nonlinear coupling between ionic transport and electric potential distribution. Such nanochannels also serve as platforms for power generation and self-powered sensing applications [191–194].

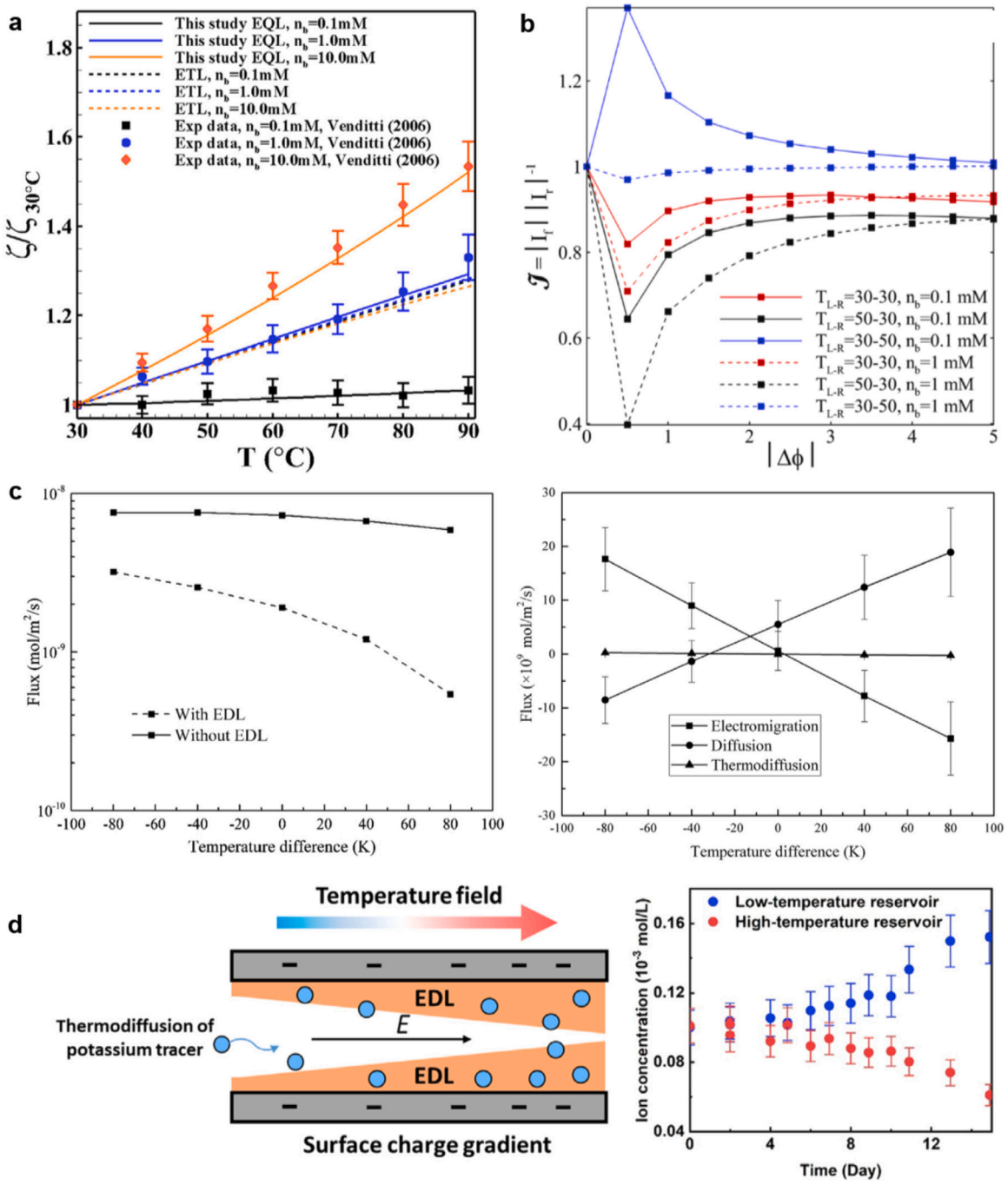

Fig. 8. (a) The zeta potential versus temperature predicted by the electrical quad layer (EQL) model for different bulk ion concentrations [149] compared with the experimental data [150] (b) Ionic flux ratio $\mathcal{J}$ of the forward and reverse currents regulated by temperature gradients in a tapered nanofluidic channel [184]. (c) The total tracer flux with or without EDL considered (left) and the flux components in clay at pore scale for different temperature gradients [185] (right). (d) Potassium concentrations in the reservoirs on both sides after applying a temperature different [186].

A thorough understanding of thermal effects on ion transport in compacted clay is crucial for ensuring the long-term safety of high-level radioactive waste repositories and other environmental applications [180]. It is observed that the macroscopic Soret coefficient in clay is five times greater than in free water, which may be attributed to electrokinetic effects [185]. Pore-scale LBM simulations reveal that the Soret effect contributes minimally to ionic flux variations in clay, as the Soret coefficient remains comparable to that of free water across different external temperature gradients (Fig. 8(c)). The primary mechanism stems from temperature-gradient-induced inhomogeneities at charged liquid–solid interfaces, which significantly alter internal electrical and concentration fields. Recently, cation thermodiffusion in saturated nanoporous silica was investigated using experimental through-diffusion methods (Fig. 8(d)) [186]. Both experimental and theoretical results demonstrate that temperature-induced surface charge polarization critically influences ionic transport by modifying the electric field within nanoconfined electrolytes under varying temperature gradients. The ionic flux is expressed using the average quantities

$$j_i^{**} = -\frac{\bar{D}_{i,0}}{GL}\left[\Delta n_i + \bar{n}_i \ln\left(\frac{n_i(T_{\text{out}})}{n_i(T_{\text{in}})}\right) + \bar{S}_T \bar{n}_i \left(T_{\text{out}} - T_{\text{in}}\right)\right], \tag{25}$$

where $n_i^* \equiv n_i/n_{i,b}^r = z_i\rho/2 + \sqrt{(\rho/2)^2+1}$ is obtained using the Donnan theory together with the local charge balance with the dimensionless volume charge density $\rho = -Q/FC_0^r$. When the EDL thickness approaches nanopore dimensions, theoretical predictions indicate that this non-isothermal ionic mobility can exceed classical thermophoretic mobility by up to an order of magnitude.

4. Electrokinetic transport in unsaturated porous media: effect of soft interface

The study of electrokinetic effects on fluid flows and ion transport in unsaturated porous media is still in its infancy. The two-liquid interface, as a typical soft interface, may allow for ion partition and distribution potential when some organic ions exist, and it will deform and flow (or even break) under external stress, opening novel opportunities in rational regulation of multiphase flow and ionic transport in micro- and nanoscales. In this section, we will summarize the primary studies on the liquid–liquid interface charging and wettability alteration effects, which are two representatives of the most important components of electrokinetic effects in micro- and nano-scale multiphase systems. The former is closely related to the interfacial charge and surface tension regulation of liquid–liquid interfaces, while the latter is primarily associated with the disjoining pressure between charged liquid–liquid and solid–liquid interfaces. More details on the electrokinetic transport at liquid–liquid interface can be found in our previous review paper [26,27].

In order to present a quantitative and predictable description of the electrokinetic transport in unsaturated porous media, the situations are quite distinct whether the electric field is present or not. When the electric field is absent, the ion-mediated multiphase flow with effective modeling ion-tuned wettability alteration is numerically simulated, which is commonly met in the low-salinity waterflooding process. When an electrical field is present, the simulation of electrokinetic transport in a multiphase system is quite challenging because of the multiscale nature of the system, and there is still a lack of study, for which we introduce the GPU-based LB simulation methods which serve as a potential candidate for the future study on the electrokinetic multiphase flow in porous media.

4.1. Liquid–liquid interface charging and electroosmosis

Surface charging at immiscible liquid–liquid interfaces plays a crucial role in emulsion stability, surfactant adsorption, and engineering applications, including drug delivery and mineral flotation. Although droplet electrophoresis serves as a common electrokinetic method for measuring surface charge density, it faces limitations in both physical modeling and sample preparation. The streaming potential, a classic electrokinetic phenomenon, arises when a pressure-driven flow transports net interfacial charges, generating convective currents that accumulate downstream in open-circuit conditions. This not only creates a difference in electrical potential that converts mechanical energy to electricity, but also enables mechanical-to-electrical signal transduction, finding diverse applications in geological and biological sensing.

Recently, a novel experimental approach of interface charging measurement is developed using a streaming-potential-based setup [195] (Fig. 9(a)). This design employs a Y-Y-shaped microchannel to establish a flat, stable liquid–liquid interface, with polymer-coated inner walls to minimize solid–liquid electrokinetic interference (Figs. 9(b–c)). The method was first validated by revisiting the aqueous solution-silicon surface charging, followed by investigation of the surfactant-free decane-KCl solution interface charging. The results confirm negative surface charging at the decane-KCl interface, with the charge magnitude increasing at higher pH values. These findings support the proposed charging mechanism, in which hydroxyl ion adsorption generates the observed negative surface charge.

Spontaneous charging at liquid–liquid interfaces often arises from imbalanced ion partitioning, particularly in polar oil systems containing large organic ions. The diffuse nature of these interfaces critically influences their electrokinetic behavior, where the interplay between different charging mechanisms is strongly dependent on interfacial physicochemical properties which are frequently overlooked in previous studies, leading to unreliable electrokinetic predictions. Recently, a novel diffuse interface framework incorporating a modified Boltzmann formulation is developed to account for solvent mixing effects and unify both charging mechanisms [197], where the additional free energy term $g(\phi)$ denoting the interaction between ions and solvents is incorporated into the equation of ion transport as an extra external force,

$$\boldsymbol{j}_i^{**} - n_i\boldsymbol{u} = -D_{i,0}\nabla n_i - z_i e b_{i,0} n_i \nabla\varphi - n_i \frac{D_{i,0}}{k_B T}\nabla g(\phi). \tag{26}$$

Here, ϕ is the order parameter denoting the relative position to the phase interface, whose evolution can be captured using the Cahn–Hilliard phase field model.

The diffuse interface model above highlights significant permittivity- and viscosity-related solvent mixing effects when imbalanced ion partitioning dominates, especially under large viscosity ratios. Through a comprehensive analysis of permittivity-dependent ion partitioning and organic impurity effects (Fig. 9(e)), they reveal distinct behaviors for polar versus non-polar organic liquids. Notably, in moderately polar organic liquids, water velocity exhibits non-monotonic dependence on impurity concentration across different pH values, reflecting competition between charging mechanisms. The authors propose a semi-empirical correction to sharp interface models to address prediction deviations, while demonstrating the crucial role of viscosity interpolation in interpreting electroosmotic velocity profiles.

4.2. Electrochemical alteration of wettability

Wettability alteration is a common approach to regulate multiphase flow in microchannels or porous media. Basically, there are two major categories in terms of electrochemical ways: one is through external voltage, which is called electrowetting (EW) [20,198,199], and the other is through spontaneous charging, which is called ion-tuned wettability alteration [24,200]. The former is a well-known phenomenon in which the contact angle of a droplet on a solid surface can be reduced by applying an electric field, and is frequently used in droplet manipulation in microfluidics, while the latter is recognized as a promising method for enhancing oil recovery by low-salinity waterflooding [24,25].

Molecular simulations are essential for elucidating ion-tuned wettability and electrowetting mechanisms because of their ability to capture discrete particle effects near the three-phase contact line and within potential water films. As we discussed in Section 2, the long-range nature of Coulombic interactions poses significant computational challenges for molecular simulations. An advanced P^3M algorithm is developed by combining precise particle–particle (PP) treatment of short-range Coulomb and van der Waals interactions and efficient particle-mesh (PM) calculation of long-range interactions, achieving both accuracy and computational efficiency. Fig. 10(a) shows the strategy of P^3M algorithm [53].

Using the above high-efficiency MD method, researchers are able to clarify the electrowetting physics and the mechanisms of voltage saturation of electrowetting (Fig. 10(b)) [54]. The simulations revealed that nanoscale droplets exhibit behavior consistent with macroscopic observations: the contact angle θ follows continuum predictions at low voltages before saturating. This saturation occurs when strong local electric fields extract ions from the droplet, with the saturation threshold modifiable through temperature adjustment, screening control, or modulation of ion-fluid binding energies. Notably, the local force balance equation for θ remains valid even post-saturation, i.e.,

$$\gamma_{vs} - \gamma_{ls} - \gamma\cos\theta_R + f_{el,x} = 0, \tag{27}$$

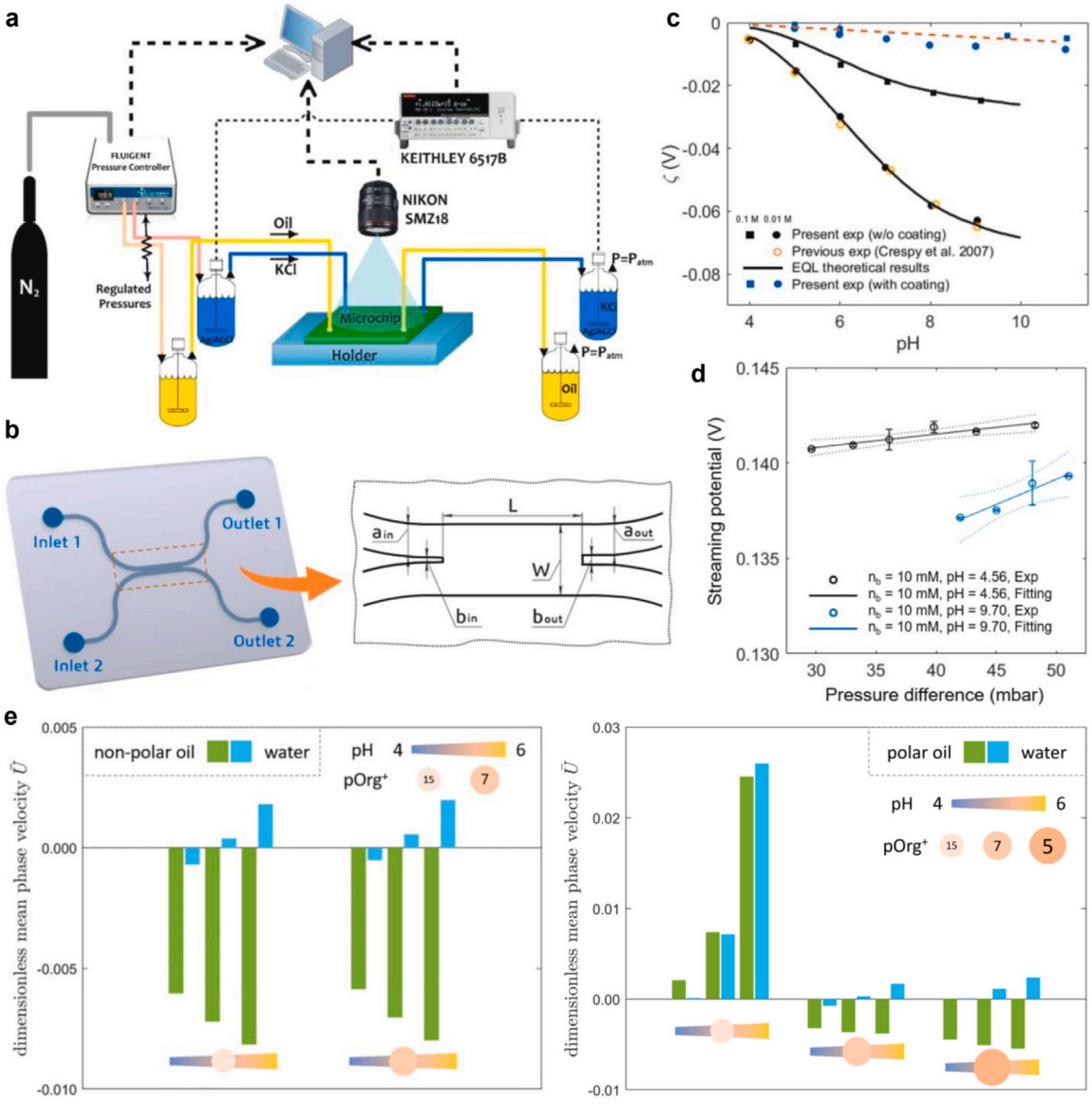

Fig. 9. (a) The experimental setup and (b) microfluidic chip design for measuring the surface charge at the oil-water interface, and (c-d) are the results from the streaming potential measurements, in which (c) is the verification of single-phase compared to the experimental data [196] and (d) the investigation of two-liquid interface [195]. (e) Dimensionless mean phase velocity in two-liquid electroosmosis for setups with different oil phases (left using non-polar oil with only ion adsorption, right using polar oil with ion partition), obtained from solving the diffuse interface model [197].

with the interface attaining its equilibrium contact angle within nanometers of the solid surface.

In ion-tuned wettability studies, the disjoining pressure serves as a fundamental parameter to quantify wettability alterations, with predictions commonly based on extended DLVO theory [24,25]. In a comprehensive theoretical investigation of ion-tuned wettability across diverse oil-brine-rock (OBR) systems, two key electrokinetic mechanisms are examined, including double layer expansion (DLE) and multicomponent ion exchange (MIE) (Fig. 10(c)) [201]. Their analysis reveals that ion-tuned wettability behavior can be categorized into two distinct types based on electrical double layer (EDL) interactions. When EDL forces are attractive, neither DLE nor MIE significantly affects water-wetness. Conversely, under repulsive EDL conditions, DLE becomes effective only at relatively high ion concentrations, whereas MIE exerts a substantially greater influence at low divalent cation percentages. Notably, the study demonstrates a synergistic interaction between DLE and MIE, where their combined effect produces significant wettability changes even when individual mechanisms show minimal impact.

Recently, a MD study on these phenomena was performed to resolve the discrete effect on ion-tuned wettability [200,203]. Their model system accurately reproduced the wettability characteristics of real oil/brine/rock systems, demonstrating qualitative agreement with EDL repulsion theory in the absence of ion-binding effects. Subsequent studies examined three fundamental mechanisms in oil-brine-quartz systems: EDL repulsion, cation bridging (Ca^{2+} and K^{+}), and hydration repulsion [202]. The molecular system contact angles and COO^{-} distributions are compared under varying interface charging conditions with EDL repulsion theory predictions, revealing that both Ca^{2+} and K^{+} bridging occur, with medium ionic strength most favorable for K^{+} bridging formation. Besides, all three mechanisms influence wettability,

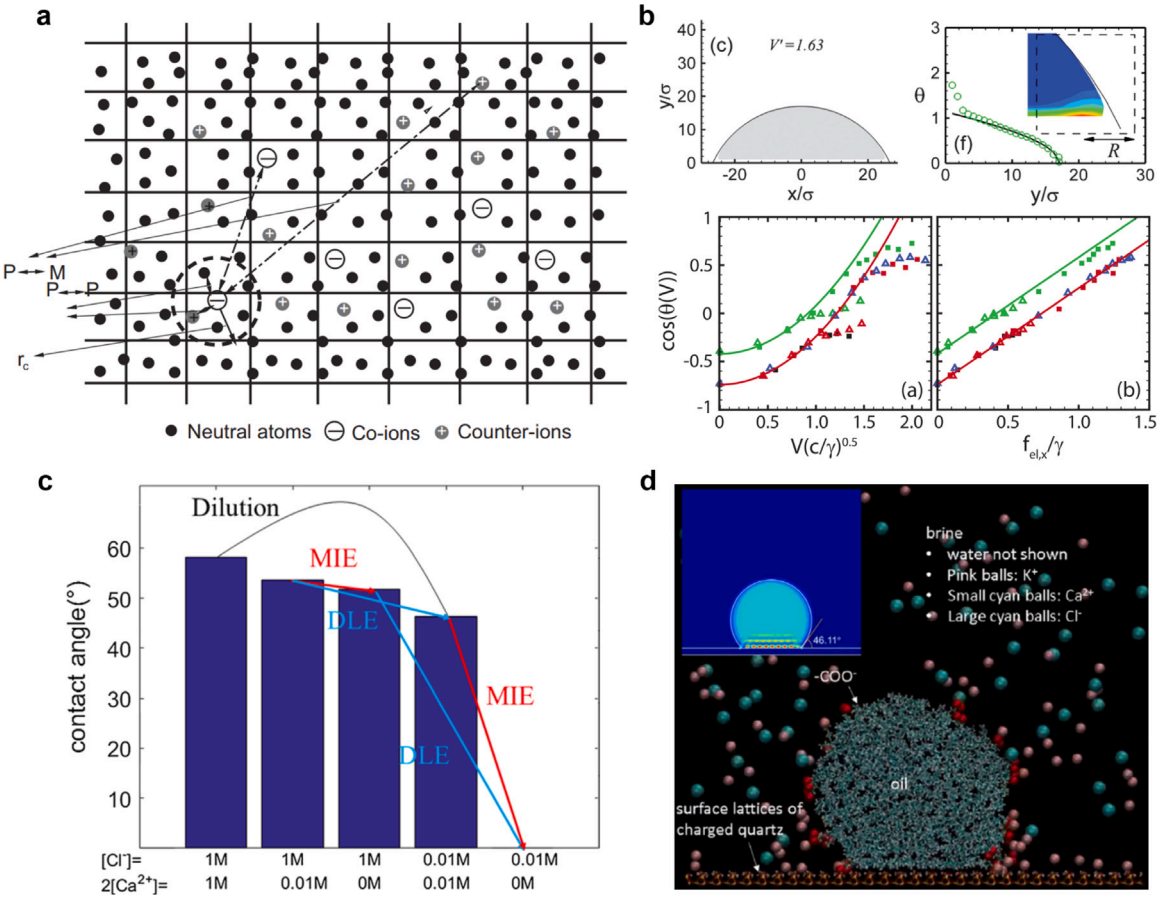

Fig. 10. (a) A two-dimensional schematic of the P^{3}M algorithm [53]. (b) Drop spreading (top) under a voltage between a cylindrical drop and electrode, and contact angle θ change (bottom) with dimensionless voltage V (or integrated electrostatic force per unit length $f_{el,x}$) [54]. γ denotes the liquid-gas interface tension coefficient. (c)Prediction of the contact angle at several different ionic compositions in ion-tuned wettability using disjoining pressure theory with surface charge regulation model, which indicate the contribution of double layer expansion (DLE) and multi-component ion exchange (MIE) [201]. (d) Schematics of MD simulation of ion-tuned wettability [200,202].

ranked by strength as: Ca^{2+} bridging > EDL repulsion ≈ hydration repulsion > K^+ bridging.

4.3. Multiphase electrokinetic flow through pores

Laboratory experiments demonstrate that oil recovery from sandstone and carbonate reservoirs during waterflooding can be significantly enhanced by modifying injected water composition, particularly through ionic strength reduction. Studies investigating dynamic wettability changes induced by surface complexation reveal substantial impacts on droplet manipulation and two-phase displacement processes [33,34,204,205]. The mobilization of trapped ganglia plays a pivotal role in two-phase displacement dynamics. Although wettability alteration represents a potential approach for ganglia mobilization, its practical feasibility and broader wettability effects have not been adequately studied.

In recent years, wettability effects on trapped ganglia have been systematically examined through theoretical analysis and numerical simulations under both fixed and dynamic wettability conditions (Fig. 11) [206], who utilized the phenomenological wettability alteration relation $\theta(c) = (\theta_1 - \theta_0)(1 + K)c/(1 + Kc) + \theta_0$ while maintaining the solute to only stay in the water phase through the constraint $c(x_w)/c_{\max} = x_w^{\lambda}$ in the recoloring step after collision in the LBM for advection–diffusion equation. Their investigation of oil-wet to water-wet transitions mediated by solute transport identified two critical mobilization mechanisms. First, initial mobilization requires heterogeneous wetting states during dynamic alteration, as step-wise changes prove ineffective. Second, sustained displacement depends on ganglia coalescence during the alteration time window - isolated ganglia exhibit only temporary mobilization before becoming trapped again upon completion of wettability alteration.

On the other hand, the presence of gas or oil (or other non-wetting and insulating phase) in the interconnected pore space significantly affects the streaming coupling coefficient. The streaming potential in multiphase displacement flow also depends on flow properties such as permeability and wettability, making it potentially useful for solving inverse problems [207,208]. For example, the self-potential generated by wet steam (quasi-uniform two-phase flow) through porous media can be significant in hydrothermal convection systems, providing a monitoring method for subsurface flow, particularly in the early stages preceding volcanic eruptions. The streaming potential in a vertical cylindrical column of porous material with wet steam flow was studied [209]. For isothermal and steady-state conditions, they observed a positive electric potential gradient along the flow direction. A sudden large increase in vapor flow rate and vapor volume fraction was found to induce a substantial and long-lasting increase in potential differences.

Early studies, including these experiments, treated the two-phase streaming potential similar to parallel single-phase flow in theoretical models [210]. Later, various modeling approaches were developed, including coarse-grained models based on volume averaging [211], simplified geometrical configurations [207], and non-equilibrium phenomenological assumptions [212–214], through which the analytical

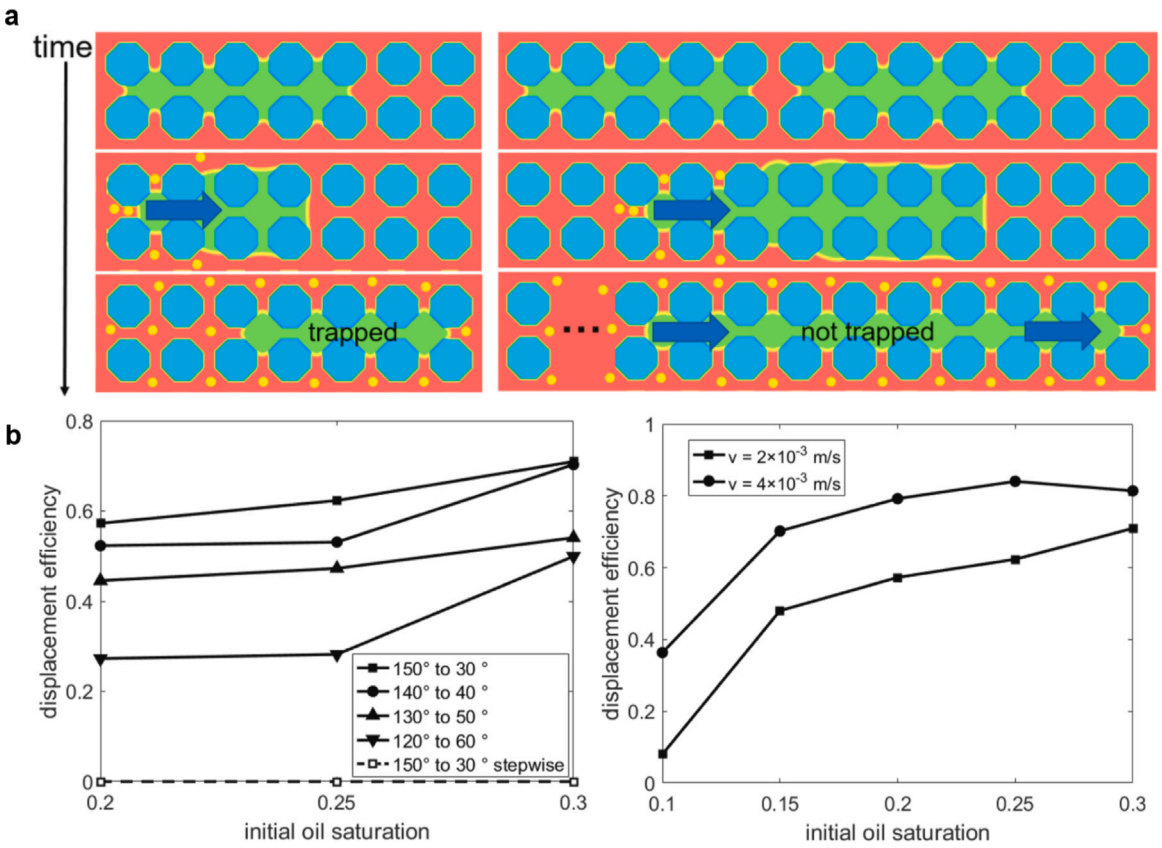

Fig. 11. (a) The evolvement of a single ganglion (left) and a group of ganglia (right) under wettability alteration by simulation. One mobilized ganglion can merge with another, extending the limited movement and growing larger. After full alteration, the ganglion can be large enough to not be trapped [206]. (b) The displacement efficiency in the irregular sandstone-like structure by displacement with solute induced wettability alteration, with varying initial oil saturation, degree of alteration (left) and inlet flow velocity v (right) [206].

models based on the capillary bundle model were proven effective and efficient despite their over-simplification of the natural complexity of geo-materials. Two main effects were considered to account for the presence of insulating phases in pores: the insulating effect itself and the negative surface charge at the fluid-liquid interfaces [215]. In addition, the effect of the distribution of the pore size on the EK coupling was further explored, and the effects of hysteresis were explained by the presence of irregularities in the pore geometry of the medium that affected the flow of water and the convection of excess surface charge [38,216,217]. However, the precise mechanisms behind these factors remained poorly understood, and the pore-scale understanding was still lacking [218,219].

Although numerical methods enable detailed tracking of interfacial phenomena, current computational frameworks face inherent limitations, particularly when external electric fields are applied or when physically realistic diffuse interface dimensions must be resolved, considering the nanoscale thickness of diffuse charge layers. Key challenges include: resolving steep concentration/electric potential gradients at interfaces, capturing large interfacial deformations, and addressing multiscale coupling effects, all of which demand substantial computational resources. These challenges share a common characteristic that significant computational costs are required to resolve critical details. Advanced mesh refinement (AMR) techniques combined with GPU computing [220,221], especially those employing dynamic adaptation, offer a promising solution to these computational bottlenecks while maintaining solution accuracy. AMR algorithms automatically adjust grid resolution based on predefined criteria, applying fine grids to critical regions (e.g., high-gradient zones) while using coarse grids elsewhere [222]. However, AMR implementations may disrupt memory address continuity, potentially reducing the efficiency of memory-block-based acceleration techniques [221,223].

In LBM implementations, uniform grids remain traditionally preferred for their algorithmic efficiency, though partial and adaptive refinement approaches are gaining adoption [224,225]. The localized computation and neighbor-dependent streaming characteristics of LBM present distinct challenges for AMR applications. Proper data transfer between coarse and fine grids requires careful rescaling of physical quantities, equilibrium distributions, and non-equilibrium components [226]. For multiphase systems, maintaining interface consistency across grid levels is particularly crucial — inadequate treatment of cross-grid interfaces or inconsistent interface thickness can compromise both accuracy and stability [227,228]. Special attention must be devoted to the rescaling process during mesh transitions in LBM implementations. Well-designed AMR strategies not only enhance the resolution of interfacial phenomena but also deliver substantial computational savings. Emerging integrations of machine learning and artificial intelligence offer promising avenues for optimizing refinement criteria selection, potentially revolutionizing both simulation efficiency and predictive accuracy in future developments.

5. Summary and perspectives

5.1. General remarks

This review paper provides a systematic summary of current progress beyond textbooks and normal research papers on electrokinetic transport within porous media from a pore-scale perspective. We focus on, but not limited to, three major fundamental effects: geometric confinement effects induced by wall structures, field inhomogeneity effects arising from coupled physicochemical processes, and soft interface effects characteristic of multiphase systems.

Specifically, we address several critical mechanisms such as discrete particle effects, complex structure effects, micro-nano junction transition, inhomogeneous surface charge distribution, surface chemical kinetics, thermodiffusion coupling, ion partitioning behavior, and dynamic wettability regulation. To highlight these complex interactions, we address several key numerical approaches, including the random generation-growth method for statistically reproducing equivalent microstructures of porous media, the lattice Poisson–Boltzmann method for simulating coupled electrokinetic transport, and particle-based methods for resolving discrete phenomena when the continuum assumption is challenged.

Although many advances and developments have been made in the past two decades, there are still many challenges and opportunities in the field of electrokinetic transport in porous media, especially for cases with multiscale, multiphysiochemical and multiphase effects. Advancing both fundamental understanding and practical applications in this field necessitates close collaboration among computational scientists, experimentalists, and theoretical researchers in the study of electrokinetic transport within complex porous systems. The expected future directions following this framework may include: (1) Development of statistics-based theoretical frameworks that integrate pore-scale electrokinetic transport physics with continuum-scale descriptions, (2) Implementation of multiscale simulation strategies that couple reactive transport processes with heterogeneous solid–fluid interactions in saturated porous media, and (3) Design of application-driven experimental platforms that enable quantitative characterization of electrokinetic phenomena in unsaturated porous media under realistic conditions.

5.2. Further exploration and perspectives

Besides the urgent demands, there would also be some potential long-term directions to be explored in the future. To be specific, the multiphase electrokinetic transport in porous media is a burgeoning field with important applications in various disciplines and industries, as shown in Fig. 1. However, the transport mechanisms are far from well understood.

On fundamental mechanism. In porous media, electrokinetic multiphase flow involves coupled hydrodynamic interactions through viscous forces and pressure gradients, arising from simultaneous electrokinetic flows at both the solid–liquid and liquid–liquid interfaces [6]. Optimizing interfacial micro-nano structures and metal electrode configurations may provide effective control strategies for such flows. For example, electrolyte displacement processes combine electrowetting with electroosmosis to influence the two-phase dynamics [25,229], which requires further theoretical analysis and numerical simulations. On the other hand, in Hele-Shaw systems, current injection could potentially suppress viscous fingering instability (occurring when a low-viscosity fluid displaces a high-viscosity one), provided that the liquid–liquid interface allows for interphase current flow [230]. However, the related experimental validations of those theories remain limited. The ion-tuned wettability governs the migration of oil droplets and the control of two-phase displacement [24]. For systems without an external electric field, ion composition/concentration primarily modulates displacement by altering contact angles [231,232]. The underlying mechanism involves ion-concentration-dependent charge regulation that modifies electrical double layer interactions. Consequently, spatio-temporal ion variations can induce dynamic wettability changes or spatial heterogeneity. In particular, the time scale for the adjustment of local wettability may match the characteristic time scales of ion transport and multiphase flows, which means that the dynamics of wettability can significantly influence two-phase flows [25]. When porous frameworks contain conductive materials, solid–liquid electrochemical reactions may further affect electrocapillary imbibition of the electrolyte, allowing active control opportunities [233].

On engineering application. Multiphase electrokinetic transport through porous media could be used as a potential solution for energy conversion and harvesting. Conventional solid–liquid streaming potentials typically lack sufficient magnitude for practical applications. As liquid–liquid interfaces permit ion slippage and enhanced charge convection, their incorporation can significantly boost streaming potential and energy conversion efficiency. In particular, the required pressure gradient needs not only originate from pumps; it can also result from solvent-atmosphere interfacial evaporation, inspired by plant transpiration [234] and later conceptualized as the hydrovoltaic effect [235,236]. Streaming potentials may thus emerge from charged liquid–liquid interfaces around droplets/bubbles [237–239], or solid–liquid interfacial processes such as chemical reactions or triboelectricity that mediate ion-electron energy exchange [240–242]. On the other side, energy and information are intrinsically linked. In groundwater monitoring, geophysicists deploy surface electrodes to measure natural streaming potential differences (self-potential method) for inferring subsurface flow patterns and multiphase interface dynamics [207,211,243]. This technique has been adapted to microfluidics, where bubble-filled nanochannels enable biofilm biochemical detection [244,245]. Recent studies reveal that lubricant composition in slippery surfaces significantly affects streaming potential generation [246], suggesting microfluidic two-phase systems could offer new approaches for quantifying liquid–liquid interfacial charging [195]. Compared with the curved interfaces of droplet electrophoresis, such planar configurations can simplify both the physical interpretation and theoretical modeling of interfacial phenomena, which requires further efforts to tackle the remaining challenges in experimental design and fabrication.

CRediT authorship contribution statement

Yunfan Huang: Writing – original draft, Investigation. **Zhiguo Tian:** Resources, Data curation. **Hangyu Chen:** Methodology. **Wei Liu:** Validation. **Moran Wang:** Writing – review & editing, Supervision, Conceptualization.

Declaration of competing interest

The authors declare that they have no known competing financial interests or personal relationships that could have appeared to influence the work reported in this paper.

Acknowledgments

This work was financially supported by National Natural Science Foundation of China (No. 12432013, 12272207, 91634107, 51676107, 51176089). The authors would like to thank previous members of the Multiscale Interfacial Transport laboratory including Dr. L. Zhang, Dr. A. Alizadeh, Dr. Y. Yang, Dr. H. Tian, Dr. F. Liu, and the anonymous referee who provided useful and detailed comments on the manuscript.

Data availability

No data was used for the research described in the article.

References

[1] Hunter RJ, Ottewill RH, Rowell RL. Zeta potential in colloid science. Principles and applications. Academic Press; 1981.
[2] Lyklema J. Solid-liquid interfaces. In: Fundamentals of interface and colloid science, Vol. II, Academic Press; 1995.
[3] Stone H, Stroock A, Ajdari A. Engineering flows in small devices: Microfluidics toward a lab-on-a-chip. Annu Rev Fluid Mech 2004;36:381–411.
[4] Squires TM, Quake SR. Microfluidics: Fluid physics at the nanoliter scale. Rev Mod Phys 2005;77(3):977–1026.
[5] Schoch RB, Han J, Renaud P. Transport phenomena in nanofluidics. Rev Mod Phys 2008;80(3):839–83.
[6] Zembala M. Electrokinetics of heterogeneous interfaces. Adv Colloid Interface Sci 2004;112:59–92.

[7] Marbach S, Bocquet L. Osmosis, from molecular insights to large-scale applications. Chem Soc Rev 2019;48(11):3102–44.
[8] Heiranian M, Fan H, Wang L, Lu X, Elimelech M. Mechanisms and models for water transport in reverse osmosis membranes: history, critical assessment, and recent developments. Chem Soc Rev 2023;52(24):8455–80.
[9] Gallo A, Sprocati R, Rolle M, Sethi R. Electrokinetic delivery of permanganate in clay inclusions for targeted contaminant degradation. J Contam Hydrol 2022;251:104102.
[10] Head NA, Gerhard JI, Inglis AM, Nunez Garcia A, Chowdhury AI, Reynolds DA, de Boer CV, Sidebottom A, Austrins LM, Eimers J, O'Carroll DM. Field test of electrokinetically-delivered thermally activated persulfate for remediation of chlorinated solvents in clay. Water Res 2020;183:116061.
[11] Sprocati R, Flyvbjerg J, Tuxen N, Rolle M. Process-based modeling of electrokinetic-enhanced bioremediation of chlorinated ethenes. J Hazard Mater 2020;397:122787.
[12] Revil A, Jardani A. The self-potential method: theory and applications in environmental geosciences. Cambridge: Cambridge University Press; 2013, p. iii.
[13] Dao V-D, Vu NH, Dang H-LT, Yun S. Recent advances and challenges for water evaporation-induced electricity toward applications. Nano Energy 2021;85:105979.
[14] Zhou J, Gu Y, Liu P, Wang P, Miao L, Liu J, Wei A, Mu X, Li J, Zhu J. Development and evolution of the system structure for highly efficient solar steam generation from zero to three dimensions. Adv Funct Mater 2019;29(50):1903255.
[15] Tan J, Fang S, Zhang Z, Yin J, Li L, Wang X, Guo W. Self-sustained electricity generator driven by the compatible integration of ambient moisture adsorption and evaporation. Nat Commun 2022;13(1):3643.
[16] Xu T, Ding X, Cheng H, Han G, Qu L. Moisture-enabled electricity from hygroscopic materials: A new type of clean energy. Adv Mater 2023;n/a(n/a):2209661.
[17] Bockris JO, Reddy AKN, Gamboa-Aldeco M. Modern electrochemistry 2A: Fundamentals of electrodics. New York: Springer; 2000.
[18] Newman J, Balsara NP. Electrochemical systems. John Wiley & Sons; 2021.
[19] Ramos A. In: Electrokinetics and electrohydrodynamics in microsystems, vol. 530, Springer Science & Business Media; 2011.
[20] Mugele F, Heikenfeld J. Electrowetting: fundamental principles and practical applications, John Wiley & Sons; 2019.
[21] Alizadeh A, Hsu W-L, Wang M, Daiguji H. Electroosmotic flow: From microfluidics to nanofluidics. Electrophoresis 2021;42(7–8):834–68.
[22] Gu Z, Xu B, Huo P, Su M, Deng D. Electroconvection instability and shocks in complex geometries. Curr Opin Colloid Interface Sci 2022;60:101604.
[23] Morrow NR. Interfacial phenomena in petroleum recovery. In: Surfactant science series, vol. 36, New York and Basel: Marcel Dekker; 1990.
[24] Tian H, Wang M. Electrokinetic mechanism of wettability alternation at oil-water-rock interface. Surf Sci Rep 2017;72(6):369–91.
[25] Liu F, Wang M. Review of low salinity waterflooding mechanisms: Wettability alteration and its impact on oil recovery. Fuel 2020;267:117112.
[26] Huang Y, Wang M. Electrokinetics at liquid-liquid interfaces: Physical models and transport mechanisms. Adv Colloid Interface Sci 2025;342:103518.
[27] Huang Y, Wang M. Electrokinetics multiphase hydrodynamics. Appl Phyiscs Rev 2025;12:031322.
[28] Wang S, Yang X, Wu F, Min L, Chen X, Hou X. Inner surface design of functional microchannels for microscale flow control. Small 2020;16(9):1905318.
[29] Guo Z, Boylan D, Shan L, Dai X. Hydrophilic reentrant SLIPS enabled flow separation for rapid water harvesting. Proc Natl Acad Sci 2022;119(36):e2209662119.
[30] Dai H, Dong Z, Jiang L. Directional liquid dynamics of interfaces with superwettability. Sci Adv 2020;6(37):eabb5528.
[31] Ramadan BS, Sari GL, Rosmalina RT, Effendi AJ, Hadrah. An overview of electrokinetic soil flushing and its effect on bioremediation of hydrocarbon contaminated soil. J Environ Manag 2018;218:309–21.
[32] Cameselle C, Gouveia S. Electrokinetic remediation for the removal of organic contaminants in soils. Curr Opin Electrochem 2018;11:41–7.
[33] Maes J, Geiger S. Direct pore-scale reactive transport modelling of dynamic wettability changes induced by surface complexation. Adv Water Resour 2018;111:6–19.
[34] An S, Zhan Y, Mahani H, Niasar V. Kinetics of wettability alteration and droplet detachment from a solid surface by low-salinity: A lattice-Boltzmann method. Fuel 2022;329:125294.
[35] Aziz R, Niasar V, Erfani H, Martínez-Ferrer PJ. Impact of pore morphology on two-phase flow dynamics under wettability alteration. Fuel 2020;268:117315.
[36] Voytek EB, Barnard HR, Jougnot D, Singha K. Transpiration- and precipitation-induced subsurface water flow observed using the self-potential method. Hydrol Process 2019;33(13):1784–801.
[37] Stroock AD, Pagay VV, Zwieniecki MA, Michele Holbrook N. The physicochemical hydrodynamics of vascular plants. Annu Rev Fluid Mech 2014;46(Volume 46, 2014):615–42.
[38] Hu K, Huang Q, Han P, Zhang Y, Mo C, Li S, Jougnot D. Characterization of rainwater infiltration within a controlled experiment by self-potential monitoring and modeling. J Hydrol 2025;660:133348.
[39] Grahame DC. The electrical double layer and the theory of electrocapillarity. Chem Rev 1947;41(3):441–501.
[40] Wang M, Chen S. On applicability of Poisson-Boltzmann equation for micro- and nanoscale electroosmotic flows. Commun Comput Phys 2008;3:1087–99.
[41] Wang M, Pan N. Predictions of effective physical properties of complex multiphase materials. Mater Sci Eng: R: Rep 2008;63(1):1–30.
[42] Tian H, Zhang L, Wang M. Applicability of donnan equilibrium theory at nanochannel–reservoir interfaces. J Colloid Interface Sci 2015;452:78–88.
[43] Liu W, Huang Y, Wang M. Extended space charge and transport near ion-selective surfaces. Int J Mech Sci 2025;287:109933.
[44] Yang Y, Patel RA, Churakov SV, Prasianakis NI, Kosakowski G, Wang M. Multiscale modeling of ion diffusion in cement paste: electrical double layer effects. Cem Concr Compos 2019;96:55–65.
[45] Yang Y, Wang M. Upscaling scheme for long-term ion diffusion in charged porous media. Phys Rev E 2017;96(2):023308.
[46] Wang M, Liu J, Chen S. Electric potential distribution in nanoscale electroosmosis: from molecules to continuum. Mol Simul 2008;34(5):509–14.
[47] Wang M, Kang Q. Modeling electrokinetic flows in microchannels using coupled lattice Boltzmann methods. J Comput Phys 2010;229(3):728–44.
[48] Allen M, Tildesley D. Computer simulation of liquids. Oxford: Clrendon Press; 1987.
[49] Wang M, J. L, Chen S. Similarity of electroosmotic flows in nanochannels. Mol Simul 2007;33(3):239–44.
[50] Qiao R, Aluru N. Ion concentrations and velocity profiles in nanochannel electroosmotic flows. J Chem Phys 2003;118:4692–701.
[51] Beckers JVL, Lowe CP, De Leeuw SW. An iterative PPPM method for simulating Coulombic systems on distributed memory parallel computers. Mol Simul 1998;20(6):369–83.
[52] Pollock E, Glosli J. Comments on P3M, FMM, and the ewald method for large periodic Coulombic systems. Comput Phys Comm 1996;95:93–110.
[53] Liu J, Wang M, Chen S, Robbins MO. Molecular simulations of electroosmotic flows in rough nanochannels. J Comput Phys 2010;229(20):7834–47.
[54] Liu J, Wang M, Chen S, Robbins MO. Uncovering molecular mechanisms of electrowetting and saturation with simulations. Phys Rev Lett 2012;108(21):216101.
[55] Guo Y, Wang M. Thermodynamics of micro- and nano-scale flow and heat transfer: a mini-review. J Non-Equilib Thermodyn 2024;49:221–35.
[56] Li D. Electrokinetics in microfluidics. Oxford: Academic Press; 2004.
[57] Masliyah J, Bhattacharjee S. Electrokinetic and colloid transport phenomena. John Wiley & Sons; 2006.
[58] Hackbush W. Multi-grid methods and applications. Springer-Verlag; 1985.
[59] Shu S, Sun D, Xu J. An algebraic multigrid method for higher-order finite element discretizations. Computing 2006;77:347–77.
[60] Alizadeh A, Wang M. A generalized local grid refinement approach for modeling of multi-physicochemical transports by lattice Boltzmann method. Adv Appl Math Mech 2018;11:1–26.
[61] Chen S, Doolen G. Lattice Boltzmann method for fluid flows. Annu Rev Fluid Mech 1998;30:329–64.
[62] He X, Li N. Lattice Boltzmann simulation of electrochemical systems. Comput Phys Comm 2000;129(1):158–66.
[63] Horbach J, Frenkel D. Lattice-Boltzmann method for the simulation of transport phenomena in charged colloids. Phys Rev E 2001;64(6):061507.
[64] Li B, Kwok D. Electrokinetic microfluidic phenomena by a lattice Boltzmann model using a modified Poisson–Boltzmann equation with an excluded volume effect. J Chem Phys 2004;120:947–53.
[65] Wang J, Wang M, Li Z. Lattice Boltzmann simulations of mixing enhancement by the electro-osmotic flow in microchannels. Mod Phyiscs Lett B 2005;19:1515–8.
[66] Wang M, Wang J, Chen S, Pan N. Electrokinetic pumping effects of charged porous media in microchannels using the lattice Poisson–Boltzmann method. J Colloid Interface Sci 2006;304(1):246–53.
[67] Wang M, Pan N, Wang J, Chen S. Lattice Poisson-Boltzmann simulations of electroosmotic flows in charged anisotropic porous media. Commun Comput Phys 2007;2(6):1055–70.
[68] Wang M, Wang J, Pan N, Chen S. Mesoscopic predictions of the effective thermal conductivity for microscale random porous media. Phys Rev E 2007;75:036702.
[69] Wang M, Chen S. Electroosmosis in homogeneously charged micro- and nanoscale random porous media. J Colloid Interface Sci 2007;314(1):264–73.
[70] Wang M, Pan N. Elastic property of multiphase composites with random microstructures. J Comput Phys 2009;228:5978—-5988.
[71] Wang J, Wang M, Li Z. Lattice Poisson–Boltzmann simulations of electro-osmotic flows in microchannels. J Colloid Interface Sci 2006;296(2):729–36.
[72] Alizadeh A, Wang JK, Pooyan S, Mirbozorgi SA, Wang M. Numerical study of active control of mixing in electro-osmotic flows by temperature difference using lattice Boltzmann methods. J Colloid Interface Sci 2013;407:546–55.
[73] Alizadeh A, Zhang L, Wang M. Mixing enhancement of low-Reynolds electro-osmotic flows in microchannels with temperature-patterned walls. J Colloid Interface Sci 2014;431:50–63.

[74] Zhang L, Wang M. Modeling of electrokinetic reactive transport in micropore using a coupled lattice Boltzmann method. J Geophys Res: Solid Earth 2015;120(5):2877–90.
[75] Wang M. Structure effects on electro-osmosis in microporous media. J Heat Transf 2012;134:051020.
[76] Wang M, Wang J, Chen S. Roughness and cavitations effects on electro-osmotic flows in rough microchannels using the lattice Poisson–Boltzmann methods. J Comput Phys 2007;226(1):836–51.
[77] Wang M, Kang Q. Electrokinetic transport in microchannels with random roughness. Anal Chem 2009;81(8):2953–61.
[78] Leroy P, Maineult A. Exploring the electrical potential inside cylinders beyond the Debye–Hückel approximation: a computer code to solve the Poisson–Boltzmann equation for multivalent electrolytes. Geophys J Int 2018;214(1):58–69.
[79] Wang M, He J, Yu J, Pan N. Lattice Boltzmann modeling of the effective thermal conductivity for fibrous materials. Int J Therm Sci 2007;46:848–55.
[80] Wang M, Pan N. Modeling and prediction of the effective thermal conductivity of random open-cell porous foams. Int J Heat Mass Transfer 2007;51:1325–31.
[81] Zhao C, Yang C. Electrokinetics of non-Newtonian fluids: A review. Adv Colloid Interface Sci 2013;201:94–108.
[82] Chen S, He X, Bertola V, Wang M. Electro-osmosis of non-Newtonian fluids in porous media using lattice Poisson–Boltzmann method. J Colloid Interface Sci 2014;436:186–93.
[83] Khan MB, Sasmal C. Electro-elastic instability in electroosmotic flows of viscoelastic fluids through a model porous system. Eur J Mech B Fluids 2023;97:173–86.
[84] Zhang L, Wang M. Effects of dielectric permittivity of solid structure on electro-osmotic permeability in porous media. J Porous Media 2015;18(10):1021–9.
[85] Chai Z, Shi B. A novel lattice Boltzmann model for the Poisson equation. Appl Math Model 2008;32:2050–8.
[86] Guan Y, Yang T, Wu J. Mixing and transport enhancement in microchannels by electrokinetic flows with charged surface heterogeneity. Phys Fluids 2021;33:042006.
[87] Zhang Y, Zhang Y-M, Luo K, Yi H-L, Wu J. Electroconvective instability near an ion-selective surface: A mesoscopic lattice Boltzmann study. Phys Rev E 2022;105(5):055108.
[88] Yoon H, Kang Q, Valocchi AJ. Lattice Boltzmann-based approaches for pore-scale reactive transport. Rev Miner Geochem 2015;80(1):393–431.
[89] Luo K, Wu J, Yi H-L, Tan H-P. Lattice Boltzmann model for Coulomb-driven flows in dielectric liquids. Phys Rev E 2016;93(2):023309.
[90] Luo K, Wu J, Yi H-L, Tan H-P. Lattice Boltzmann modelling of electro-thermo-convection in a planar layer of dielectric liquid subjected to unipolar injection and thermal gradient. Int J Heat Mass Transfer 2016;103:832–46.
[91] Xu A, Shyy W, Zhao T. Lattice Boltzmann modeling of transport phenomena in fuel cells and flow batteries. Acta Mech Sin 2017;33(3):555–74.
[92] Zangle TA, Mani A, Santiago JG. Theory and experiments of concentration polarization and ion focusing at microchannel and nanochannel interfaces. Chem Soc Rev 2010;39(3):1014–35.
[93] Donnan FG. The theory of membrane equilibria. Chem Rev 1924;1(1):73–90.
[94] Teorell T. 9 - transport processes and electrical phenomena in ionic membranes. Prog Biophys Biophys Chem 1953;3:305–69.
[95] Dukhin SS. Electrokinetic phenomena of the second kind and their applications. Adv Colloid Interface Sci 1991;35:173–96.
[96] Zaltzman B, Rubinstein I. Electro-osmotic slip and electroconvective instability. J Fluid Mech 2007;579:173–226.
[97] Dydek EV, Zaltzman B, Rubinstein I, Deng DS, Mani A, Bazant MZ. Overlimiting current in a microchannel. Phys Rev Lett 2011;107(11):118301.
[98] Mani A, Wang KM. Electroconvection near electrochemical interfaces: Experiments, modeling, and computation. Annu Rev Fluid Mech 2020;52(1):509–29.
[99] Zhang L, Biesheuvel PM, Ryzhkov II. Theory of ion and water transport in electron-conducting membrane pores with pH-dependent chemical charge. Phys Rev Appl 2019;12:014039.
[100] McClure JE, Li Z. Capturing membrane structure and function in lattice Boltzmann models. Phys Rev E 2023;107:024408.
[101] Garboczi EJ, Bentz DP. Modelling of the microstructure and transport properties of concrete. Constr Build Mater 1996;10(5):293–300.
[102] Patel RA, Perko J, Jacques D, De Schutter G, Ye G, Van Bruegel K. Effective diffusivity of cement pastes from virtual microstructures: Role of gel porosity and capillary pore percolation. Constr Build Mater 2018;165:833–45.
[103] Tits J, Jakob A, Wieland E, Spieler P. Diffusion of tritiated water and 22Na+ through non-degraded hardened cement pastes. J Contam Hydrol 2003;61:45–62.
[104] Yang Y, Wang M. Cation diffusion in compacted clay: A pore-scale view. Environ Sci Technol 2019;53(4):1976–84.
[105] Yang Y, Wang M. Pore-scale modeling of chloride ion diffusion in cement microstructures. Cem Concr Compos 2018;85:92–104.
[106] Appelo C. Solute transport solved with the Nernst-Planck equation for concrete pores with 'free' water and a double layer. Cem Concr Res 2017;101:102–13.
[107] Zhang Y, Ye G, Yang Z. New insights into long-term chloride transport in unsaturated cementitious materials: Role of degree of water saturation. Constr Build Mater 2020;238:117677.
[108] Chen D, Yang K, Hu D, Shi J. A meso-stochastic research on the chloride transport in unsaturated concrete. Constr Build Mater 2021;273:121986.
[109] Liu C, Zhang M. Microstructure-based modelling of chloride diffusivity in non-saturated cement paste accounting for capillary and gel pores. Cem Concr Res 2023;168:107153.
[110] Yang Y, Patel RA, Prasianakis NI, Churakov SV, Deissmann G, Bosbach D. Elucidating the role of water films on solute diffusion in unsaturated porous media by improved pore-scale modeling. Vadose Zone J 2024;23:e20321.
[111] Yang Y, Churakov SV, Patel RA, Prasianakis N, Deissmann G, Bosbach D, Poonoosamy J. Pore-scale modeling of water and ion diffusion in partially saturated clays. Water Resour Res 2024;60(1):e2023WR035595.
[112] Sprocati R, Gallo A, Sethi R, Rolle M. Electrokinetic delivery of reactants: Pore water chemistry controls transport, mixing, and degradation. Environ Sci Technol 2021;55(1):719–29.
[113] Liu QF, Hu Z, Wang XE, Zhao H, Qian K, Li LJ, Meng Z. Numerical study on cracking and its effect on chloride transport in concrete subjected to external load. Constr Build Mater 2022;325:126797.
[114] Wu T, Yang Y, Wang Z, Shen Q, Tong Y, Wang M. Anion diffusion in compacted clays by pore-scale simulation and experiments. Water Resour Res 2020;56(11):e2019WR027037.
[115] Liu C, Zhang M. Multiscale modelling of ionic diffusivity in unsaturated concrete accounting for its hierarchical microstructure. Cem Concr Res 2022;156:106766.
[116] Xie C, Li H. Multiscale simulations of nanofluidics: Recent progress and perspective. Wiley Interdiscip Rev: Comput Mol Sci 2023;13:e1661.
[117] Liang M, Liu Y, Xiao B, Yang S, Wang Z, Han H. An analytical model for the transverse permeability of gas diffusion layer with electrical double layer effects in proton exchange membrane fuel cells. Int J Hydrog Energy 2018;43(37):17880–8.
[118] Thanh LD, Jougnot D, Do PV, Hue DT, Thuy TT, Tuyen VP. Predicting electrokinetic coupling and electrical conductivity in fractured media using a fractal distribution of tortuous capillary fractures. Appl Sci 2021;11(11).
[119] Guarracino L, Jougnot D. A fractal model for effective excess charge density in variably saturated fractured rocks. J Geophys Res: Solid Earth 2022;127(3):e2021JB022982.
[120] Jouniaux L, Bordes C. Frequency-dependent streaming potentials: A review. Int J Geophys 2012;2012(1):648781.
[121] Jougnot D, Solazzi SG. Predicting the frequency-dependent effective excess charge density: A new upscaling approach for seismoelectric modeling. GEOPHYSICS 2021;86(5):WB19–28.
[122] Gallo A, Sprocati R, Islam KT, Rolle M. Combined effects of porosity, tortuosity and pore water composition on electrokinetic transport dynamics in porous media. Electrochim Acta 2025;524:145969.
[123] Xie Q, Zheng D, Geng Z, Deng J, Wen Z, Li G, Zhang F. Synergistic heating and electrokinetic effects of direct current electric fields: numerical modeling of multi-field coupling for contaminant removal in heterogeneous porous media. J Hydrol 2025;662:134066.
[124] Sprocati R, Gallo A, Wienkenjohann H, Rolle M. Temperature-dependent dynamics of electrokinetic conservative and reactive transport in porous media: A model-based analysis. J Contam Hydrol 2023;259:104261.
[125] Liu J, Wang D, Kvetny M, Brown W, Li Y, Wang G. Quantification of steady-state ion transport through single conical nanopores and a nonuniform distribution of surface charges. Langmuir 2013;29(27):8743–52.
[126] Brown W, Kvetny M, Yang R, Wang G. Higher ion selectivity with lower energy usage promoted by electro-osmotic flow in the transport through conical nanopores. J Phys Chem C 2021;125(6):3269–76.
[127] Lin C-Y, Wong P-H, Wang P-H, Siwy ZS, Yeh L-H. Electrodiffusioosmosis-induced negative differential resistance in pH-regulated mesopores containing purely monovalent solutions. ACS Appl Mater Interfaces 2020;12(2):3198–204.
[128] Davis J, James R, Leckie J. Surface ionization and complexation at the oxide/water interface: I. Computation of electrical double layer properties in simple electrolytes. J Colloid Interface Sci 1978;63:480–99.
[129] Davis J, Leckie J. Surface ionization and complexation at the oxide/water interface II. Surface properties of amorphous iron oxyhydroxide and adsorption of metal ions. J Colloid Interface Sci 1978;67:90–107.
[130] Hsu W, Daiguji H, Dunstan D, Davidson M, Harvie D. Electrokinetics of the silica and aqueous electrolyte solution interface: Viscoelectric effects. Adv Colloid Interface Sci 2016;234:108–31.
[131] Behrens S, Grier D. The charge of glass and silica surfaces. J Chem Phys 2001;115:6716–21.
[132] Stein D, Kruithof M, Dekker C. Surface-charge-governed ion transport in nanofluidic channels. Phys Rev Lett 2004;93:035901.
[133] Wang M, Kang Q, Eli B-N. Modeling of electrokinetic transport in silica nanofluidic channels. Anal Chim Acta 2010;664:158–64.
[134] Wang M, Kang Q. Electrochemomechanical energy conversion efficiency in silica nanochannels. Microfluid Nanofluidics 2010;9:181–90.
[135] Zhang L, Wang M. Electro-osmosis in inhomogeneously charged microporous media by pore-scale modeling. J Colloid Interface Sci 2017;486:219–31.

[136] Gaudin A, Fuerstenau D. Quartz flotation with anionic collectors. Trans Am Inst Min Met Eningeers 1955;202:66–72.
[137] Gaudin A, Fuerstenau D. Quartz flotation with cationic collectors. Trans Am Inst Min Met Eningeers 1955;202:958–62.
[138] Glover PW, Déry N. Streaming potential coupling coefficient of quartz glass bead packs: Dependence on grain diameter, pore size, and pore throat radius. GEOPHYSICS 2010;75(6):F225–41.
[139] Zhang J, Vinogradov J, Leinov E, Jackson MD. Streaming potential during drainage and imbibition. J Geophys Res: Solid Earth 2017;122(6):4413–35.
[140] Kormiltsev VV, Ratushnyak AN, Shapiro VA. Three-dimensional modeling of electric and magnetic fields induced by the fluid flow movement in porous media. Phys Earth Planet Inter 1998;105(3):109–18.
[141] Revil A, Leroy P. Constitutive equations for ionic transport in porous shales. J Geophys Res: Solid Earth 2004;109(B3). http://dx.doi.org/10.1029/2003JB002755.
[142] Duan C, Majumdar A. Anomalous ion transport in 2-nm hydrophilic nanochannels. Nature Nanotechnology 2010;5:848–52.
[143] Hunter R. The significance of stagnant layer conduction in electrokinetics. Adv Colloid Interface Sci 2003;100:153–67.
[144] Lyklema J. Quest for ion-ion correlations in electric double layers and overcharging phenomena. Adv Colloid Interface Sci 2009;147:205–13.
[145] Wang M, Revil A. Electrochemical charge of silica surfaces at high ionic strength in narrow channels. J Colloid Interface Sci 2010;343(1):381–6.
[146] Gonçalvès J, Rousseau-Gueutin P, Revil A. Introducing interacting diffuse layers in TLM calculations: A reappraisal of the influence of the pore size on the swelling pressure and the osmotic efficiency of compacted bentonites. J Colloid Interface Sci 2007;316(1):92–9.
[147] Charmas R, Piasecki W, Rudzinski W. 4-layer complexation model for ion adsorption at electrolyte/oxide interface - theoretical foundations. Langmuir 1995;11:3199–210.
[148] Alizadeh A, Wang M. Flexibility of inactive electrokinetic layer at charged solid-liquid interface in response to bulk ion concentration. J Colloid Interface Sci 2019;534:195–204.
[149] Alizadeh A, Wang M. Temperature effects on electrical double layer at solid-aqueous solution interface. Electrophoresis 2020;41(12):1067–72.
[150] Venditti R, Xuan X, Li D. Experimental characterization of the temperature dependence of zeta potential and its effect on electroosmotic flow velocity in microchannels. Microfluid Nanofluidics 2006;2:493–9.
[151] Zhang L. Multiphysicochemical ion transport in microporous media [Ph.D. thesis], Tsinghua University; 2018.
[152] Zhang L, McNeece CJ, Hesse MA, Wang M. Reactive transport of protons in electro-osmotic displacements with electrolyte concentration difference in a microcapillary. Anal Chem 2018;90(20):11802–11.
[153] Alizadeh A, Wang M. Direct simulation of electroosmosis around a spherical particle with inhomogeneously acquired surface charge. Electrophoresis 2017;38(5):580–95.
[154] Wang M, Kang Q, Viswanathan H, Robinson BA. Modeling of electro-osmosis of dilute electrolyte solutions in silica microporous media. J Geophys Res: Solid Earth 2010;115:B10205.
[155] Eykholt GR, Daniel DE. Impact of system chemistry on electroosmosis in contaminated soil. J Geotech Eng 1994;120:797–815.
[156] Wang YD, Meyer Q, Tang K, McClure JE, White RT, Kelly ST, Crawford MM, Iacoviello F, Brett DJL, Shearing PR, Mostaghimi P, Zhao C, Armstrong RT. Large-scale physically accurate modelling of real proton exchange membrane fuel cell with deep learning. Nat Commun 2023;14:745.
[157] Dukhin AS, Xu R. Electric double layer models. Interface Sci Technol 2025;39:9–69.
[158] Aseyednezhad S, Yan L, Hassanizadeh SM, Raoof A. An accurate reduced-dimension numerical model for evolution of electrical potential and ionic concentration distributions in a nano-scale thin aqueous film. Adv Water Resour 2022;159:104058.
[159] Zhang L, Wang M. Theoretical analysis of reverse electrodialysis in nanochannel. J Eng Thermophys 2015;36:154–7.
[160] Alizadeh A, Wang M. Reverse electrodialysis through nanochannels with inhomogeneously charged surfaces and overlapped electric double layers. J Colloid Interface Sci 2018;529:214–23.
[161] Alizadeh A, Jin X, Wang M. Pore-scale study of ion transport mechanisms in inhomogeneously charged nanoporous rocks: Impacts of interface properties on macroscopic transport. J Geophys Res: Solid Earth 2019;124(6):5387–407.
[162] Hsu JP, Chen YM, Yang ST, Lin CY, Tseng S. Influence of salt valence on the rectification behavior of nanochannels. J Colloid Interface Sci 2018;531:483–92.
[163] Alizadeh A, Daiguji H, Benneker AM. A theoretical understanding of ionic current through a nanochannel driven by a viscosity gradient. J Colloid Interface Sci 2022;628:545–55.
[164] Jiao Y, Yang C, Zhang W, Wang Q, Zhao C. A review on direct osmotic power generation: Mechanism and membranes. Renew Sustain Energy Rev 2024;191:114078.
[165] Zhang Z, Li Z, Shi Y, Chen X, Qiao N, Li C. The synergistic effects of salinity and pressure gradients on sustainable energy conversion in nanofluidics. Desalination 2024;586:117885.
[166] Muniruzzaman M, Rolle M. Modeling multicomponent ionic transport in groundwater with IPhreeqc coupling: Electrostatic interactions and geochemical reactions in homogeneous and heterogeneous domains. Adv Water Resour 2016;98:1–15.
[167] Muniruzzaman M, Rolle M. Multicomponent ionic transport modeling in physically and electrostatically heterogeneous porous media with PhreeqcRM coupling for geochemical reactions. Water Resour Res 2019;55(12):11121–43.
[168] Lyklema J, Minor M. On surface conduction and its role in electrokinetics. Colloids Surfaces A: Physicochem Eng Asp 1998;140(1–3):33–41.
[169] Kang Q, Wang M, Mukherjee PP, Lichtner PC. Mesoscopic modeling of multiphysicochemical transport phenomena in porous media. Adv Mech Eng 2010;2:142879.
[170] Zhang L, Hesse MA, Wang M. Dispersion of charged solute in charged micro- and nanochannel with reversible sorption. Electrophoresis 2019;40(6):838–44.
[171] Zhang L, Hesse MA, Wang M. Transient solute transport with sorption in Poiseuille flow. J Fluid Mech 2017;828:733–52.
[172] Rodríguez-Romo S, Ibañez-Orozco O. Two-dimensional lattice Boltzmann for reactive Rayleigh–Bénard and Bénard–Poiseuille regimes. 17, (10):2015, p. 6698–711.
[173] Song H, Wang Y, Wang J, Li Z. Unifying diffusion and seepage for nonlinear gas transport in multiscale porous media. Chem Phys Lett 2016;661:246–50.
[174] Xu Q, Long W, Jiang H, Zan C, Huang J, Chen X, Shi L. Pore-scale modelling of the coupled thermal and reactive flow at the combustion front during crude oil in-situ combustion. Chem Eng J 2018;350:776–90.
[175] Liu R, Yao S, Li Y, Cheng J. Pore-scale study of dynamic ion adsorption process in porous electrodes of capacitive deionization using lattice Boltzmann method. Int J Heat Mass Transfer 2019;135:769–81.
[176] Li H, Clercx HJH, Toschi F. Lattice Boltzmann method investigation of a reactive electro-kinetic flow in porous media: towards a phenomenological model. Philos Trans R Soc A: Math Phys Eng Sci 2021;379(2208):20200398.
[177] Yang P, Ye S, Wu J, Wu J. Process-based pore-scale simulation of electrokinetic remediation of organic pollutant in porous media. J Hydrol 2022;613:128436.
[178] Soldi M, Guarracino L, Jougnot D. Predicting streaming potential in reactive media: the role of pore geometry during dissolution and precipitation. Geophys J Int 2024;236(2):967–78.
[179] Liu R, Yao S, Shen Y. Pore-scale investigation on ion transport and transfer resistance in charged porous media with micro-macro structure. J Mol Liq 2020;320:114481.
[180] Yan H, Sedighi M, Xie H. Thermally induced diffusion of chemicals under steady-state heat transfer in saturated porous media. Int J Heat Mass Transfer 2020;153:119664.
[181] Song Z, Hao Y, Liu H. Analytical study of the thermo-osmosis effect in porothermoelastic responses of saturated porous media under axisymmetric thermal loadings. Comput Geotech 2020;123:103576.
[182] Chen WQ, Jivkov AP, Sedighi M. Thermo-osmosis in charged nanochannels: Effects of surface charge and ionic strength. ACS Appl Mater Interfaces 2023;15(28):34159–71.
[183] Zhang W, Farhan M, Jiao K, Qian F, Guo P, Wang Q, Yang CC, Zhao C. Simultaneous thermoosmotic and thermoelectric responses in nanoconfined electrolyte solutions: Effects of nanopore structures and membrane properties. J Colloid Interface Sci 2022;618:333–51.
[184] Alizadeh A, Hsu W-L, Daiguji H, Wang M. Temperature-regulated surface charge manipulates ionic current rectification in tapered nanofluidic channel. Int J Mech Sci 2021;210:106754.
[185] Yang Y, Wang M. Pore-scale study of thermal effects on ion diffusion in clay with inhomogeneous surface charge. J Colloid Interface Sci 2018;514:443–51.
[186] Yang Y, Zhang X, Tian Z, Deissmann G, Bosbach D, Liang P, Wang M. Thermodiffusion of ions in nanoconfined aqueous electrolytes. J Colloid Interface Sci 2022;619:331–8.
[187] Qiao N, Li Z, Zhang Z, Guo H, Liao J, Lu W, Li C. Effect of membrane thermal conductivity on ion current rectification in conical nanochannels under asymmetric temperature. Anal Chim Acta 2023;1278:341724.
[188] Xu H, Zheng X, Shi X. Surface hydrophilicity-mediated migration of nano/microparticles under temperature gradient in a confined space. J Colloid Interface Sci 2023;637:489–99.
[189] Eden A, Pennathur S. Coupling charge-regulated interfacial chemistry to electrokinetic ion transport in bipolar SiO2-Al2O3 nanofluidic diodes. Adv Mater Interfaces 2024;11(35):2400495.
[190] Farhan M, Zhang W, Wang Q, Zhao C. Asymmetric thermo-electro-osmotic responses in charged conical nanochannels. Int Commun Heat Mass Transfer 2024;159:108128.
[191] Xiao T, Li X, Liu Z, Lu B, Zhai J, Diao X. Low-cost 2D nanochannels as biomimetic salinity- and heat-gradient power generators. Nano Energy 2022;103:107782.
[192] Pan J, Xu W, Zhang Y, Ke Y, Dong J, Li W, Wang L, Wang B, Meng B, Zhou Q, Xia F. Osmotic energy-based systems for self-powered sensing. Nano Energy 2024;132:110412.
[193] Zhang Y, Guo S, Yu ZG, Qu H, Sun W, Yang J, Suresh L, Zhang X, Koh JJ, Tan SC. An asymmetric hygroscopic structure for moisture-driven hygro-ionic electricity generation and storage. Adv Mater 2022;34(21):2201228.

[194] Glatzel F, Janssen M, Härtel A. Reversible heat production during electric double layer buildup depends sensitively on the electrolyte and its reservoir. J Chem Phys 2021;154(6):064901.
[195] Alizadeh A, Huang Y, Liu F, Daiguji H, Wang M. A streaming-potential-based microfluidic measurement of surface charge at immiscible liquid-liquid interface. Int J Mech Sci 2023;247:108200.
[196] Crespy A, Boleve A, Revil A. Influence of the dukhin and Reynolds numbers on the apparent zeta potential of granular porous media. J Colloid Interface Sci 2007;305:188–94.
[197] Huang Y, Wang M. Solvent mixing and ion partitioning effects in spontaneous charging and electrokinetic flow of immiscible liquid-liquid interface. Phys Rev Fluids 2024;9(10):103701.
[198] Welters W, Fokkink L. Fast electrically switchable capillary effects. Langmuir 1998;14:1535–8.
[199] Hayes R, Feenstra B. Video-speed electronic paper based on electrowetting. Nature 2003;425:383–5.
[200] Tian H, Wang M. Molecular dynamics for ion-tuned wettability in oil/brine/rock systems. AIP Adv 2017;7(12):125017.
[201] Liu F, Wang M. Electrokinetic mechanisms and synergistic effect on ion-tuned wettability in oil-brine-rock systems. Transp Porous Media 2021;140(1):7–26.
[202] Tian H, Liu F, Jin X, Wang M. Competitive effects of interfacial interactions on ion-tuned wettability by atomic simulations. J Colloid Interface Sci 2019;540:495–500.
[203] Pan B, Yin X, Iglauer S. A review on clay wettability: From experimental investigations to molecular dynamics simulations. Adv Colloid Interface Sci 2020;285:102266.
[204] Abu-Al-Saud MO, Esmaeilzadeh S, Riaz A, Tchelepi HA. Pore-scale study of water salinity effect on thin-film stability for a moving oil droplet. J Colloid Interface Sci 2020;569:366–77.
[205] Norouzisadeh M, Leroy P, Soulaine C. A lubrication model with slope-dependent disjoining pressure for modeling wettability alteration. Comput Phys Comm 2024;298:109114.
[206] Liu F, Wang M. Wettability effects on mobilization of ganglia during displacement. Int J Mech Sci 2022;215:106933.
[207] Jackson MD. Multiphase electrokinetic coupling: Insights into the impact of fluid and charge distribution at the pore scale from a bundle of capillary tubes model. J Geophys Res: Solid Earth 2010;115:B07206.
[208] Jackson MD, Vinogradov J. Impact of wettability on laboratory measurements of streaming potential in carbonates. Colloids Surfaces A: Physicochem Eng Asp 2012;393:86–95.
[209] Antraygues P, Aubert M. Self potential generated by two-phase flow in a porous medium: Experimental study and volcanological applications. J Geophys Res: Solid Earth 1993;98(B12):22273–81.
[210] Sprunt ES, Mercer TB, Djabbarah NF. Streaming potential from multiphase flow. Geophysics 1994;59(5):707–11.
[211] Revil A, Linde N, Cerepi A, Jougnot D, Matthäi S, Finsterle S. Electrokinetic coupling in unsaturated porous media. J Colloid Interface Sci 2007;313(1):315–27.
[212] Guichet X, Jouniaux L, Pozzi J-P. Streaming potential of a sand column in partial saturation conditions. J Geophys Res: Solid Earth 2003;108(B3):2141.
[213] Revil A, Cerepi A. Streaming potentials in two-phase flow conditions. Geophys Res Lett 2004;31(11):L11605.
[214] Saunders JH, Jackson MD, Pain CC. A new numerical model of electrokinetic potential response during hydrocarbon recovery. Geophys Res Lett 2006;33:L15316.
[215] Revil A, Schwaeger H, Cathles III L, Manhardt P. Streaming potential in porous media - 2. Theory and application to geothermal system. J Geophys Research-Part B-Solid Earth-Printed Ed 1999;104(9):20033–48.
[216] Jougnot D, Mendieta A, Leroy P, Maineult A. Exploring the effect of the pore size distribution on the streaming potential generation in saturated porous media, insight from pore network simulations. J Geophys Res: Solid Earth 2019;124(6):5315–35.
[217] Soldi M, Guarracino L, Jougnot D. An effective excess charge model to describe hysteresis effects on streaming potential. J Hydrol 2020;588:124949.
[218] Wurmstich B, Morgan FD. Modeling of streaming potential responses caused by oil well pumping. Geophysics 1994;59(1):46–56.
[219] Linde N, Jougnot D, Revil A, Matthäi SK, Arora T, Renard D, Doussan C. Streaming current generation in two-phase flow conditions. Geophys Res Lett 2007;34(3):L03306.
[220] Bank RE, Sherman AH, Weiser A. Some refinement algorithms and data structures for regular local mesh refinement. Sci Comput Appl Math Comput Phys Sci 1983;1:3–17.
[221] Yang G, Chen Y, Chen S, Wang M. Implementation of a direct-addressing based lattice Boltzmann GPU solver for multiphase flow in porous media. Comput Phys Comm 2023;291:108828.
[222] Berger MJ, Colella P. Local adaptive mesh refinement for shock hydrodynamics. J Comput Phys 1989;82(1):64–84.
[223] Valero-Lara P. Leveraging the performance of LBM-hpc for large sizes on GPUs using ghost cells. In: International conference on algorithms and architectures for parallel processing. Springer; 2016, p. 417–30.
[224] Watanabe S, Aoki T. Large-scale flow simulations using lattice Boltzmann method with AMR following free-surface on multiple GPUs. Comput Phys Comm 2021;264:107871.
[225] Hsu F-S, Chang K-C, Smith M. Multi-block adaptive mesh refinement (AMR) for a lattice Boltzmann solver using GPUs. Comput & Fluids 2018;175:48–52.
[226] Lagrava D, Malaspinas O, Latt J, Chopard B. Advances in multi-domain lattice Boltzmann grid refinement. J Comput Phys 2012;231(14):4808–22.
[227] Leclaire S, Pellerin N, Reggio M, Trépanier J-Y. An approach to control the spurious currents in a multiphase lattice Boltzmann method and to improve the implementation of initial condition. Internat J Numer Methods Fluids 2015;77(12):732–46.
[228] Tölke J, Freudiger S, Krafczyk M. An adaptive scheme using hierarchical grids for lattice Boltzmann multi-phase flow simulations. Comput & Fluids 2006;35(8–9):820–30.
[229] Siddiqui MAQ, Sadeghinezhad E, Regenauer-Lieb K, Roshan H. Electrolytic flow in partially saturated charged micro-channels: Electrocapillarity vs electro-osmosis. Phys Fluids 2022;34(11):112001.
[230] Mirzadeh M, Bazant MZ. Electrokinetic control of viscous fingering. Phys Rev Lett 2017;119(17):174501.
[231] Sheng JJ. Critical review of low-salinity waterflooding. J Pet Sci Eng 2014;120:216–24.
[232] Tetteh JT, Brady PV, Barati Ghahfarokhi R. Review of low salinity waterflooding in carbonate rocks: mechanisms, investigation techniques, and future directions. Adv Colloid Interface Sci 2020;284:102253.
[233] Pan B, Valappil MO, Rateick R, Clarkson CR, Tong X, Debuhr C, Ghanizadeh A, Birss VI. Hydrophobic nanoporous carbon scaffolds reveal the origin of polarity-dependent electrocapillary imbibition. Chem Sci 2023;14(6):1372–85.
[234] Borno RT, Steinmeyer JD, Maharbiz MM. Charge-pumping in a synthetic leaf for harvesting energy from evaporation-driven flows. Appl Phys Lett 2009;95(1):013705.
[235] Zhang Z, Li X, Yin J, Xu Y, Fei W, Xue M, Wang Q, Zhou J, Guo W. Emerging hydrovoltaic technology. Nature Nanotechnology 2018;13(12):1109–19.
[236] Wang X, Lin F, Wang X, Fang S, Tan J, Chu W, Rong R, Yin J, Zhang Z, Liu Y, Guo W. Hydrovoltaic technology: from mechanism to applications. Chem Soc Rev 2022;51(12):4902–27.
[237] Sherwood JD, Xie Y, van den Berg A, Eijkel JCT. Theoretical aspects of electrical power generation from two-phase flow streaming potentials. Microfluid Nanofluidics 2013;15(3):347–59.
[238] Fiorentino E-A, Toussaint R, Jouniaux L. Lattice Boltzmann modelling of streaming potentials: variations with salinity in monophasic conditions. Geophys J Int 2016;205(1):648–64.
[239] Leroy P, Jougnot D, Revil A, Lassin A, Azaroual M. A double layer model of the gas bubble/water interface. J Colloid Interface Sci 2012;388(1):243–56.
[240] Yin J, Zhang Z, Li X, Zhou J, Guo W. Harvesting energy from water flow over graphene? Nano Lett 2012;12(3):1736–41.
[241] Coquinot B, Bocquet L, Kavokine N. Hydroelectric energy conversion of waste flows through hydroelectronic drag. Proc Natl Acad Sci 2024;121(43):e2411613121.
[242] Song D, Zhao C, Chen B, Ma W, Wang K, Zhang X. Conveyor mode enabling continuous ionic thermoelectric conversion. Joule 2024;3217–32.
[243] Revil A, Finizola A, Gresse M. Self-potential as a tool to assess groundwater flow in hydrothermal systems: A review. J Volcanol Geotherm Res 2023;437:107788.
[244] Ma Y, Sun M, Duan X, van den Berg A, Eijkel JCT, Xie Y. Dimension-reconfigurable bubble film nanochannel for wetting based sensing. Nat Commun 2020;11(1):814.
[245] Yao Y, Bennett RKA, Xu Y, Rather AM, Li S, Cheung TC, Bhanji A, Kreder MJ, Daniel D, Adera S, Aizenberg J, Wang X. Wettability-based ultrasensitive detection of amphiphiles through directed concentration at disordered regions in self-assembled monolayers. Proc Natl Acad Sci 2022;119(43):e2211042119.
[246] Fan B, Bhattacharya A, Bandaru PR. Enhanced voltage generation through electrolyte flow on liquid-filled surfaces. Nat Commun 2018;9(1):4050.